2018-09-04

Thalamic Nuclei Localization Using fMRI for Image-Guided Thalamotomy in Movement Disorders

Shie, Nancy

UNIVERSITY OF CALGARY

Thalamic Nuclei Localization Using fMRI for Image-Guided Thalamotomy in Movement Disorders

by

Nancy Shie

A THESIS

SUBMITTED TO THE FACULTY OF GRADUATE STUDIES

IN PARTIAL FULFILMENT OF THE REQUIREMENTS FOR THE

DEGREE OF MASTER OF SCIENCE

GRADUATE PROGRAM IN BIOMEDICAL ENGINEERING

CALGARY, ALBERTA

SEPTEMBER, 2018

ABSTRACT

Thalamotomy and deep brain stimulation (DBS) are important surgical options for patients with tremor-dominant movement disorders. They have provided significant improvements to those with Parkinson's disease (PD), essential tremor (ET), and dystonic tremor (DT) in their daily quality of life. Both neurosurgery techniques require presurgical imaging to localize targets for electrode placement. The thalamus is a common target for patients with uncontrollable tremor. It is made up of multiple, irregularly shaped nuclei with vague and almost indistinguishable topographies (Sommer, 2003). Improving the localization of these nuclei prior to electrode implantation can potentially reduce surgery times and increase success rates. The use of magnetic resonance imaging (MRI) allows us to study soft tissue structures, such as the brain, noninvasively, with high resolution, and without using ionizing radiation. More recently, the functional activity and connections within the brain can be visualized using MRI sequences that detect signals highly correlated with neuronal activity, a technique called functional MRI (fMRI). In this thesis we aimed to localize specific thalamic nuclei using fMRI, by looking at task-based activations (TB-fMRI) and functional connections in the resting state (RS-fMRI), between the thalamus and the sensory and motor cortices in ET and tremor-dominant PD patients, as well as in healthy controls. Results showed that TB-fMRI and RS-fMRI each localized the motor regions of the thalamus to >10mm from expected motor thalamus locations obtained from surgical lesion locations and literature reported locations. There were no differences in localized motor thalamus locations between groups using either fMRI technique. However, the motor thalamus was more distinctly separated from the sensory thalamus using TB-fMRI. This may ultimately result in a more accurate thalamic mapping process prior to thalamic lesioning or DBS electrode implantation, shorten resulting surgical times and improve overall surgical outcome.

PREFACE

This thesis is original, unpublished, independent work by the author, N. Shie. The data collection and subsequent analysis in Chapters 5, 6, and 7 were covered by Ethics Certificate #2003-25, SADA 2002/1 fMRI, issued by McGill University Health Center Research Ethics Board (NEUPSY Panel) under the original project title ‘fMRI Topography of the Thalamus in Normal Subjects and Patients with Thalamic lesions’.

ACKNOWLEDGEMENTS

Thank you first and foremost to my supervisor, Dr. Bruce Pike, for his endless patience, guidance, and support. Not only did he provide my primary source of funding for this project but has also allowed me to partake in learning opportunities abroad which I would not have been able to do otherwise. Thank you for continuously being there to answer all my questions.

Acknowledgements also extend to the rest of the Calgary lab group. Thank you to Erin Mazerolle, Jean-Sebastien Provost, Rebecca Williams, and Ethan MacDonald for teaching me about neuroimaging methods, validating my choice of statistical tests, checking my work, and editing this thesis. Thank you to Kristin and Christa for your always exceptional organization and coordination, as well as the constant supply of coffee. Credit must also be given to the lab members in Montreal for the original data collection: Halleh Ghaderi, Dr. Abbas Sadikot, Ayça Altinkaya and Dr. Jennifer Campbell. Thank you also to the NSERC CREATE i3t program and the Cumming School of Medicine Research Enhancement Program for providing additional external sources of funding.

Thank you to my parents, my friends locally or elsewhere, and my favourite roommate Justin for all current and ongoing emotional support, always believing in my everchanging goals (academic or otherwise) and letting me complain whenever I want. Lastly, a shout out to Christopher Columbus for bringing the cacao bean back to Europe so they could make it better by refining it with added sugar.

TABLE OF CONTENTS

LIST OF TABLES

LIST OF FIGURES

LIST OF SYMBOLS AND ABBREVIATIONS

AC	anterior commissure
ANCOVA	analysis of covariance
ANOVA	analysis of variance
BA	Brodmann's Area
BET	brain extraction tool
BOLD	blood-oxygen level dependent
CBF	cerebral blood flow
CI	confidence interval
$CMRO_2$	cerebral metabolic rate of oxygen
CSF	cerebral spinal fluid
CT	computed tomography
cZI	caudal zona incerta
DBS	deep brain stimulation
dHb	deoxyhemoglobin
DMN	default mode network
DRT	dentate-rubro-thalamic
DTI	diffusion tensor imaging
EPI	echo planar imaging
ET	essential tremor
FAST	FMRIB's Automated Segmentation Tool
FDR	false discovery rate
FLAME	FMRIB's Local Analysis of Mixed Effects
FLIRT	FMRIB's Linear Image Registration Tool
FNIRT	FMRIB's Non-linear Image Registration Tool
G_f	frequency encoding gradient
G_p	phase encoding gradient
G_{ss}	slice select gradient
GABA	gamma amino-butyric acid
GLM	general linear model
GPi	globus pallidus internal
GRE	gradient recalled echo
HRF	hemodynamic response function
ICA	independent component analysis
M_0	main magnetic field vector
M1	primary motor cortex
MMSE	Mini Mental State Examination
MRI	magnetic resonance imaging
MRgFUS	magnetic resonance-guided focused ultrasound
PD	Parkinson's Disease
PET	positron emission tomography
PC	posterior commissure
PMC	premotor cortex

RF	radiofrequency
ROI	region of interest
RS-fMRI	resting-state functional magnetic resonance imaging
S1	primary somatosensory cortex
SE	spin echo
SMA	supplementary motor area
SNR	signal to noise ratio
T1w	T_1-weighted
TB-fMRI	task-based functional magnetic resonance imaging
TE	echo time
TR	repetition time
UPDRS	United Parkinson's Disease Rating Scale
Vim	ventral intermediate nucleus
Vo	ventral oralis
Vop	ventral oralis posterior
VPL	ventral posterolateral nucleus
VPM	ventral posteromedial nucleus

CHAPTER 1: **INTRODUCTION**

Magnetic resonance imaging (MRI) is a diverse medical imaging modality that can be utilized with various acquisition sequences to yield different information. The advances made in the field of MR technology have had a tremendous impact on diagnostic healthcare and presurgical imaging for neurosurgical applications. MRI is frequently used clinically to look at brain structure but can also be used to measure concentrations of certain metabolites, assess the magnetic properties of tissue, and map brain connectivity. MRI sequences can also be used to detect activation in the brain, with a method known as functional magnetic resonance imaging (fMRI).

FMRI has become one of the most common functional imaging tools for presurgical planning in areas of neurosurgery such as tumor resection (Miner, 2017). FMRI can guide the surgeon by identifying critical areas of the brain that should be avoided to minimize functional deficits. Furthermore, fMRI can show changes in the brain activity following the creation of a lesion or resection of a tumour. More recently, fMRI has been adapted to help surgeons target subcortical areas necessary for thalamotomies or deep brain stimulation (DBS) – both important surgeries for the treatment of many movement disorders such as Parkinson's Disease (PD) and essential tremor (ET). Advances in surgeries targeting the subcortical areas have driven the need for better targeting techniques.

The fMRI data analyzed in this thesis is only a subset of a larger study encompassing various other MR image types, including diffusion data looking at structural white matter tracts in the brain, and magnetization transfer images sensitive to the macromolecular content of white matter. In the complete data set, the patients scanned have various tremor dominant movement disorders and are all candidates for neurosurgical intervention. The participant pool includes patients with PD, ET, and dystonic tremor, as well as a comparable healthy participant group.

Many of the patients also have longitudinal post-surgical scans. The purpose of this larger study is to further understand the pathology behind tremor-dominant movement disorders, how to optimise surgical treatment, and the effects of thalamic surgical intervention.

This thesis uses the functional and structural MRIs to better understand how fMRI can identify and locate specific surgical targets in the brain. The next chapter will provide background information; introducing the pathology of these movement disorders and relevant physiology, as well as a brief explanation of the physical mechanisms underlying MRI and fMRI acquisition and analysis methods. Chapter 3 will focus on reviewing the current literature related to MRI-based thalamic targeting. This will include a discussion of diffusion and fMRI methods, and limitations of current targeting techniques. This will lead to Chapter 4, which will focus on the hypothesis driving this thesis. Chapter 5 will present the methods used in this study and discuss the rationale for their usage. Results presented in Chapter 6 will explain the outcomes from fMRI based thalamic localization. Following this, Chapter 7 will discuss the physiological and methodological rationale that underlies many of results found in this study. This chapter will also cover some the issues confounding the results, and potential work to be done in the future. Lastly, Chapter 8 will summarize the findings within this thesis.

CHAPTER 2: **BACKGROUND**

2.1 Principles of Movement Disorders – Physiology and Pathology

Movement disorders are among the most common chronic neurological diseases. With an increasing life expectancy, the occurrence of movement disorders has increased globally and has become a concern for health care systems. Epidemiological studies project that the prevalence of various movement disorders will increase considerably between 2010 to 2050. In some countries, the number of Parkinson's Disease (PD) patients are expected to double by 2050, with an even greater increase of dementia associated with PD (Bach, Ziegler, Deuschl, Dodel, & Doblhammer-Reiter, 2011). Parkinson's disease is currently estimated to be affecting 7 million people worldwide. A recent report showed that this resulted in over 100 000 deaths in 2013 (Murray, 2015). This makes PD the second most fatal neurodegenerative disorder in the world, following Alzheimer's disease.

To understand the potential treatments for these movement disorders, it is important to understand the relevant neuroanatomy and physiology, and to consider the disease etiology relating to each individual patient.

2.1.1 Movement Disorders

Movement disorders are generally defined by dyskinesia, which are abnormal and involuntary movements, and is usually caused by nervous system dysfunction, specifically in the areas of the brain associated with movement initiation, control, and regulation. Tremors are a characteristic seen in many movement disorders, including but not exclusive to PD, essential tremor (ET), and dystonia; tremors may also be present in non-movement neurological disorders, such as stroke and multiple sclerosis (A. Benabid et al., 1996; Larson, 2014). Dyskinesia can range

from small trembling in the hands to dramatic jerks and large shaking movements in the arms, head, face, trunk, legs, and/or vocal cords (Deuschl et al., 1998; Larson, 2014).

Of the aforementioned movement disorders, PD is perhaps the most widely known and discussed. Although the exact etiology of PD is not known, it is thought to have a variety of causes. Many, if not all cases of PD can be attributed to varying amounts of genetic influence (Singleton, Farrer, & Bonifati, 2013). Often, this genetic component is affected by environmental factors (Braak & Del Tredici, 2008). It is well accepted that PD can be pathologically characterized by the appearance of Lewy bodies within the brain stem, and the degeneration of dopaminergic neurons from the substantia nigra pars compacta to the striatal motor loci, resulting in the clinical motor symptoms recognizable as PD (Gibrat et al., 2009). Despite these concrete histological changes within the brain, patients manifest a wide variety of clinical symptoms broadly categorized as parkinsonism, with PD as the most common form of parkinsonism. This may also be referred to as "idiopathic parkinsonism". Clinical symptoms include resting tremor, rigidity, bradykinesia and freezing, postural instability, and a flexed posture (Jankovic, 2008). Disease progression also varies between patients. In some patients, symptoms occur at the initial PD diagnosis, but may also eventually disappear. Other patients will experience a gradual worsening of symptoms (Duval, Daneault, Hutchison, & Sadikot, 2016). These symptoms are clinically characterized using an established scale called the Unified Parkinson's Disease Rating Scale (UPDRS), which provides a survey of both motor and non-motor elements of PD (Goetz et al., 2007; Jankovic, 2008). Other neurodegenerative disorders may also manifest with parkinsonism features and include such as progressive supranuclear palsy and corticobasal degeneration. These symptoms are generally referred to as "atypical parkinsonism" (Larson, 2014). However, subjects exhibiting these symptoms have been excluded from this study.

A second movement disorder characterized predominantly by tremor is appropriately named essential tremor (ET). It constitutes one of the most common neurological diseases worldwide, affecting 4% of people above the age of 40, and up to 20% of the population over 90 years of age (Louis & Ferreira, 2010). While ET has no single etiology, it is commonly associated with a variety of different genetic mutations (Deng, Le, & Jankovic, 2007; Shahed & Jankovic, 2007). Although generally characterized by action tremor, rather than resting tremor as in PD, studies have shown that both diseases share many of the same clinical symptoms, including both action and resting tremors in some cases (Shahed & Jankovic, 2007; Thenganatt & Jankovic, 2016). While clinical symptoms of ET tend to also include postural, head, and voice tremors, which are less common in PD patients, the overlap of clinical symptoms makes the disentanglement of ET and PD diagnoses difficult. The relationship between the diseases has been controversial and is debated in the literature. It has been found that patients diagnosed with ET may be predisposed to developing PD in the future, however, these cases are still controversial and remain open to interpretation (Shahed & Jankovic, 2007). Pathologically, neuroimaging studies have shown similar dopaminergic deficits and the development of similar Lewy body pathologies in both disorders, although this certainly is not the case in all ET patients (Deng et al., 2007; Papavassiliou et al., 2004). The link between PD and ET is a controversial finding, and such findings may indicate the presence of a "PD-ET" syndrome to add to the already large array of motor dysfunctions (Shahed & Jankovic, 2007; Thenganatt & Jankovic, 2016). There have also been suggestions to reclassify ET as a syndrome and not a specific disease. Instead, manifestations of pure tremor has been proposed to be called primary tremor, and can be associated with any disease where tremor is present (Elble, 2013).

2.1.2 The Somatosensory and Motor Systems

The underlying implication in movement disorders is dysregulation in areas of the central nervous system controlling sensory or motor function. Generation of a motor response originates in the frontal lobe, which controls cognitive functions leading to goal-directed behaviours. The frontal lobe projects the idea of movement into the premotor cortex (PMC) to prepare for muscular orientation, and to the supplemental motor area (SMA) to plan and coordinate the future movements. Both the PMC and the SMA are located adjacent to the primary motor cortex (M1) which itself is in the precentral gyrus of the frontal lobe. Neurons of the M1 are arranged anatomically, and axons leaving the M1 remain in the same organization through the descending pathway. Mapping of the axons creates a topographical map of the body, called the motor homunculus as seen on the right side of Figure 2-1, in red (Figure 2-1B). The motor homunculus does not correspond with anatomical proportions of the body, but exaggerates muscles involved in more dextrous and agile movements, such as the fingers and the lower face. These outgoing axons of the M1 primarily projects through the corticospinal tract, through many parts of the

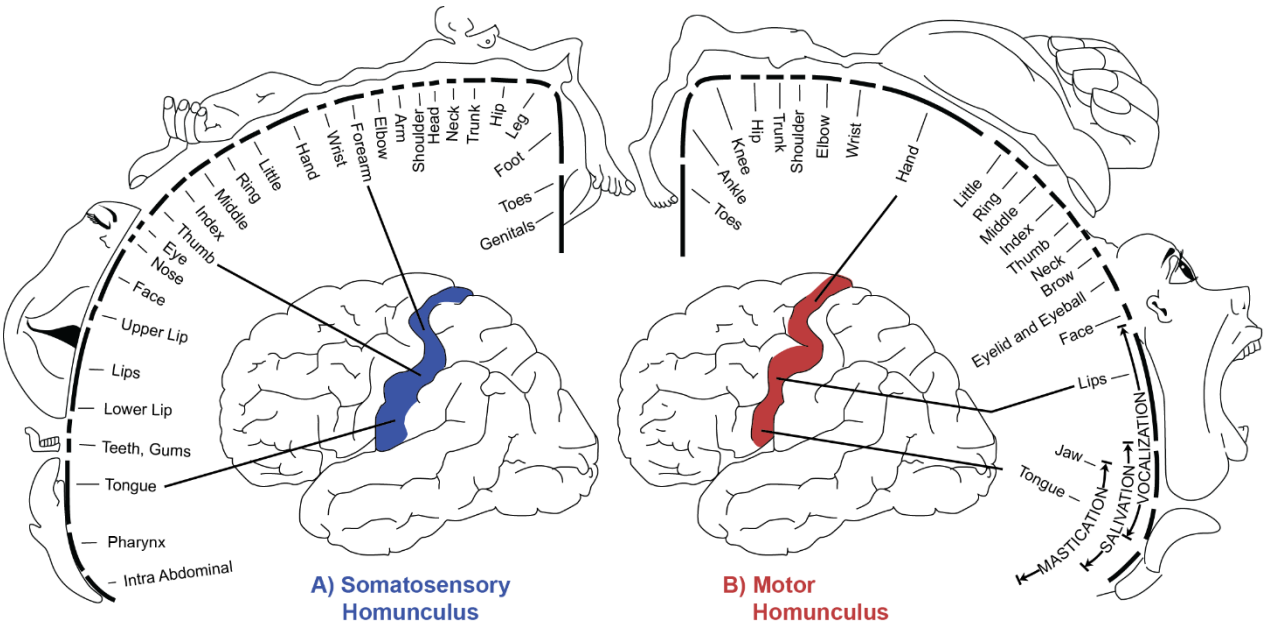

Figure 2-1: The cortical homunculi is a distorted representation of the human body as its laid out in the motor (red) and somatosensory (blue) cortices. Adapted from Barrett, Brooks, Boitano, & Barman, 2010; Komisaruk et al., 2011.

midbrain including the basal ganglia, brainstem and cerebellum, before continuing into the spinal cord.

Movements produced are heavily controlled and modulated via signals from incoming sensory inputs. Major motor and sensory afferents and efferents relaying through the thalamus are pictured in Figure 2-2A. Sensory inputs from the peripheral nerves run up the sensory pathways of the spinal cord, or through the cranial nerves if the sensory inputs originate from above the neck. Depending on the type of stimulus, these sensory inputs travel through the dorsal column system, or the spinothalamic tract, both of which relay through the thalamus. The thalamus is an important relay for modulating motor outputs. Many tracts from the thalamus travel directly to the postcentral gyrus of the cerebral cortex where the primary somatosensory cortex (S1) is located. The axons in S1 maintain the same organization throughout the pathway similar to M1, and the corresponding topographical map is called the somatosensory homunculus (Figure 2-1A). Like the motor homunculus, the somatosensory homunculus is not anatomically proportional, but designates a larger area for the more sensitive areas of the body, particularly the fingers, lips, and genitals. Other tracts from the thalamus receive signals from the cerebellum and basal ganglia before projecting to M1 to further refine motor coordination (Guyton & Hall, 2006).

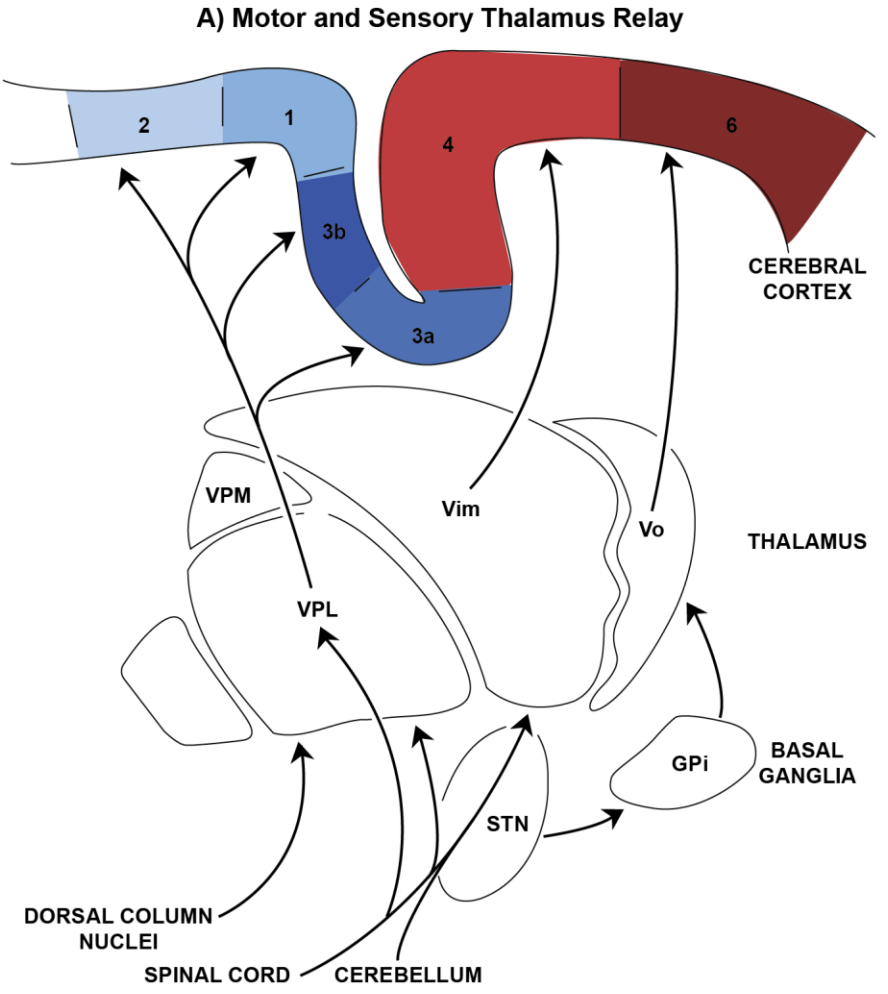
A) Motor and Sensory Thalamus Relay
2
1
3b
3a
4
6
CEREBRAL CORTEX
VPM
Vim
Vo
THALAMUS
VPL
GPi
BASAL GANGLIA
STN
DORSAL COLUMN NUCLEI
SPINAL CORD
CEREBELLUM

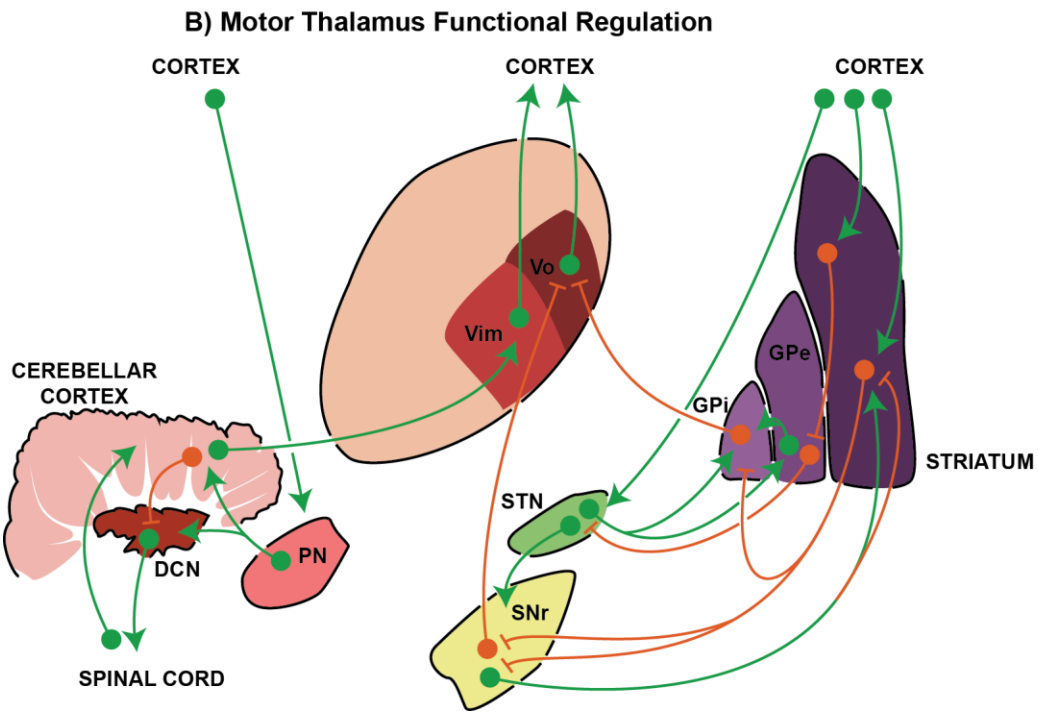
B) Motor Thalamus Functional Regulation
CORTEX
CORTEX
CORTEX
Vo
Vim
GPe
GPi
CEREBELLAR CORTEX
STRIATUM
STN
DCN
PN
SNr
SPINAL CORD

Figure 2-2: A) Major afferent and efferent tracks relaying through the thalamus. Cerebral cortex is labelled using Brodmann's areas. B) Important excitatory and inhibitory pathways in motor thalamus function as it pertains to basal ganglia and cerebellar involvement. Green pathways are excitatory, orange pathways are inhibitory. DCN: deep cerebellar nuclei, GPe: globus pallidus external, GPi: globus pallidus internal, PN: pontine nucleus, Vim: Ventral intermediate nucleus, Vo: Ventral oralis nucleus, VPL: ventral posterolateral nucleus, VPM: ventral posteromedial nucleus, SNr: substantia nigra pars reticulate, STN: Subthalamic nucleus. Adapted from Jones, 2007; Perlmutter & Mink, 2006; Yamamoto et al., 2013.

Functions of the thalamus comprise more than just motor control. The thalamus is among one of the largest organized structures in the brain, making up 1% of the whole brain volume, and contains approximately ten million neurons. Non-motor functions include sleep and consciousness regulation, visual, auditory, gustatory and visceral sensory relay, roles in spatial memory, and more. The thalamus contains over 50 anatomically and functionally distinct subnuclei which contribute to these motor and non-motor processes (Jones, 2007; Kultas-Ilinsky & Ilinskii, 2001). The thalamic subnuclei important to this thesis are highlighted are Figure 2-3.

Nuclei relating to motor and somatosensory processes are mainly housed within the ventral portion of the thalamus, as seen in Figure 2-2A. The somatosensory system uses the ventral posterior nucleus, sometimes named the ventral caudal nucleus, of the thalamus to relay signals from the cerebellum to the cortex. The ventral posterior nucleus is located between the external and internal medullary lamina of the thalamus and is posteriorly tapered towards the medial geniculate nucleus. It is well defined into two parts, the ventral posteromedial nucleus (VPM) and the ventral posterolateral nucleus (VPL). While relative sizing differs between species, the VPL is a much larger portion in humans, on account of its representation of the hands and feet (Jones, 2007). Thalamocortical tracts from the ventral posterior complex are projected mostly to Brodmann's Area 3a and 3b, although BA 3b receives a much greater density of neurons and is

typically considered the primary somatosensory cortex (S1). Both cortical areas are laid out according to the cortical homunculus (Jones, 2007; Purves et al., 2001). Numerous studies have shown that the limbs and trunk of most species is represented within the VPL, and the head and face by the VPM (Jones, 2007).

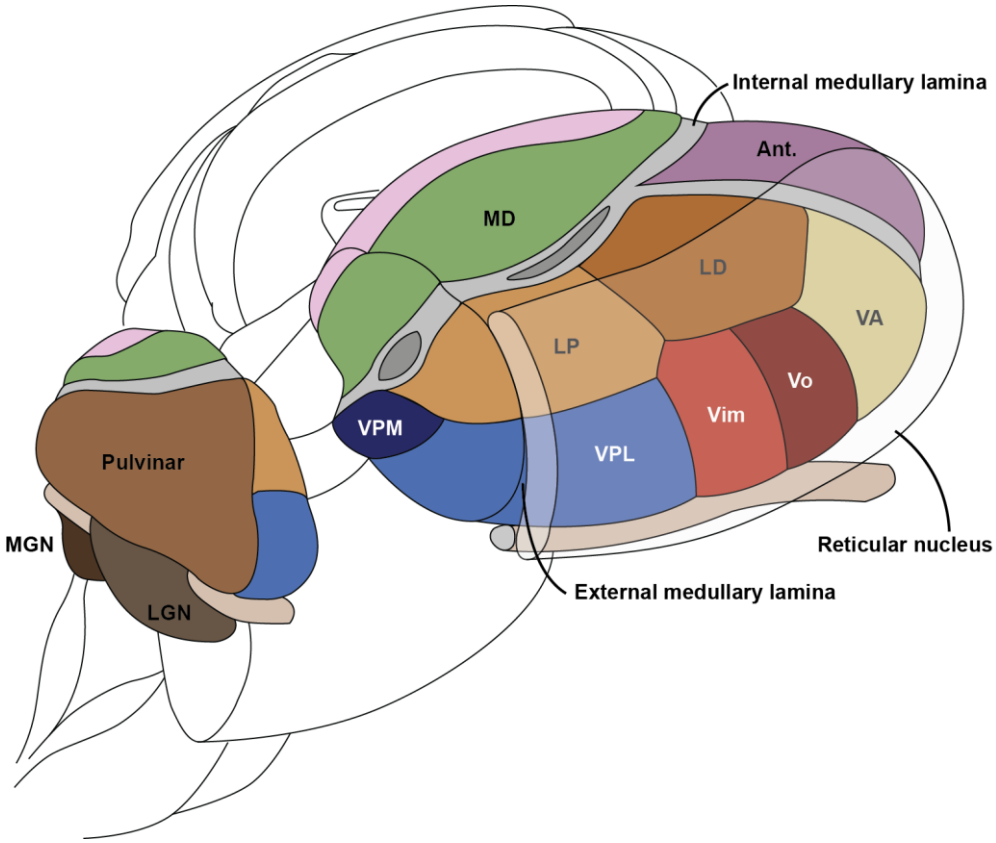

Figure 2-3: Subnuclei of the thalamus. MD: Medial dorsal nucleus, Ant: Anterior Nucleus, LD: Lateral dorsal nucleus, LP: Lateral posterior nucleus, VA: Ventral anterior nucleus, Vo: Ventral oralis nucleus, Vim: Ventral intermediate nucleus, VPL: Ventral posterior nucleus, VPM: Ventral posteromedial nucleus, LGN: Lateral geniculate nucleus, MGN: Medial geniculate nucleus. Adapted from Felten, O'Banion, & Maida, 2015.

The motor system's connections, shown in Figure 2-2A, run mainly through the ventral lateral complex. This area is made of two major subdivisions, the posterior and the anterior. The posterior division is named ventral intermediate nucleus (Vim) or the ventral lateral posterior and

is the larger of the two main subsections of the ventral lateral complex. Functionally, this area receives the majority of the afferent connections from the cerebellum. Outgoing projections from the Vim target Brodmann's area 4 of the cortex, encompassing the primary motor cortex (M1). The Vim is also further modulated by feedback loops primarily from the motor cortex and the cerebellum. These are detailed in Figure 2-2B. The other subdivision is generally known as the ventral oralis nucleus (Vo), or the ventral lateral anterior nucleus. The Vo receives inputs from the globus pallidus internal segment (GPi), and projects to Brodmann's area 6, situated anterior to M1, which make up the PMC, and the SMA. The Vo is mainly modulated by the basal ganglia pathways in both direct and indirect feedback systems. (Jones, 2007; Sommer, 2003; Vitek, Ashe, DeLong, & Alexander, 1994).

2.1.3 Treating Tremor

The appearance of tremor itself has a variable etiology between movement disorder patients. In ET patients with postural tremor, neurons within the thalamus have been shown to exhibit firing patterns at tremor frequency, but not when the subject was at rest. Within the thalamus, the Vim had the highest percentage of neurons exhibiting this characteristic, as compared to the VPL, or Vo. This may indicate that tremor associated with ET is partially modulated by voluntary neurons within the Vim (Hua, 2004). Studies in PD patients have shown a correlation between tremor-related neural activity modulated by the basal ganglia, and in the thalamic Vo, the target of basal ganglion projections in the thalamus. It is speculated that hyperactive gamma amino-butryic acid (GABA) output by the GPi in PD patients is responsible for inducing a low-threshold calcium spike activity in thalamic cells, causing these thalamic cells in the Vo to fire at rhythmic tremor frequencies (Cagnan et al., 2014; Duval et al., 2016). Because

of the variability in etiology of many of these movement disorders, one neuronal model for disease does not represent the case for all patients with the disorder. While the etiology of the tremor is important, the manifestation of all symptoms must still be considered for a systemic treatment of the pathology.

PD and ET also respond to different treatments. Dopamine deficient pathways are generally the target of most drugs used for idiopathic parkinsonism treatment, including dopamine agonists, monoamine oxidase inhibitors, and catechol-O-methyl transferase inhibitors as the most prevalent ones (Shahed & Jankovic, 2007). These drugs are generally not as effective in subjects with atypical parkinsonism (Larson, 2014). Many different drugs are also commonly accepted to treat ET, including beta blockers, anti-epileptics, benzodiazepines, and injections such as botulinum toxins. Treatment is often tailored to fit individual cases based on factors including symptoms, history with disease, and the attending clinician's experiences and preferences, as the understanding of pharmacological responsiveness towards different ET symptoms is currently limited (Zesiewicz et al., 2008).

Tremor in PD and ET patients often becomes unresponsive to medication and other therapies over time (Duval et al., 2016). When this occurs, neurosurgical intervention is often the next step to alleviate tremor. The two main therapies currently used to accomplish this goal are deep brain stimulation (DBS), and surgical ablation (for example, thalamotomy). These have both been shown to significantly affect the appearance of tremor. Non-invasive brain stimulation (for example, transcranial magnetic stimulation) is also a potentially valid treatment, however it is still in early experimental stages (Picillo et al., 2015; Rohani & Fasano, 2017), and thus will not be discussed further.

The process of DBS involves implanting an electrode in a targeted area of the brain to modulate the neural circuits in that area. The electrode is connected to an internal pulse generator to maintain a specific amplitude and frequency of stimulus. The exact modulatory effects of DBS is not completely understood, however there are both excitatory and inhibitory local effects, causing widespread changes to the targeted network (Kringelbach, Jenkinson, Owen, & Aziz, 2007; Larson, 2014). These are thought to work via various voltage-gated ion channels causing channel-dependent activation or inactivation. In patients with tremor-dominant movement disorders, the Vim is a common target for tremor alleviation neurosurgical intervention (A. Benabid et al., 1996; Perlmutter & Mink, 2006). Because the Vim acts as a relay between the deep cerebellar nuclei, other thalamic neurons, cortical motor areas, and the striatum (Perlmutter & Mink, 2006), DBS likely influences many of the upstream and downstream elements through Vim stimulation.

Another surgery for treating tremor is thalamotomy. Thalamotomies can be carried out with various tools and methods, with many recent advances in this area. A thalamotomy is an incision or an ablation of an area in the thalamus to change the function of the rest of the brain. The earliest lesions were electrolytic, however these were found to be very irregular and unpredictable. Mechanical lesions using wire loops to obtain brain core tissue became more common in the 1930s. This wire loop tool was refined further into a leucotome, which is now used to perform both mechanical lesions and biopsies. Around the same time, thermal-coagulation using high frequency currents was developed. Once greater control of current intensity, voltage, and temperature was possible, this progressed into the use of radiofrequency (RF) coagulation. Another technique using cryogenic lesion-making also became popular. Cryothalamotomies use inserted cannulas with a freezing tip to create a reversible or irreversible lesion, depending on the temperature of the cannula. Many of these, including mechanical lesioning, RF lesioning and

cryolesioning are used frequently today, while new lesioning methods have also evolved (Redfern & Ruskin, 1989). Gamma knife radiosurgery uses ionizing radiation, transmitted through the skull without highly-invasive surgery. The device focuses beams of gamma radiation from many directions, and only the center of focus receives enough radiation dose to ablate the tissue. A newer technology, called magnetic resonance-guided focused ultrasound (MRgFUS) also uses non-invasive targeting techniques, however, avoids ionizing radiation, and instead, uses focused ultrasound waves to create thermal lesions on targeted tissue (Rohani & Fasano, 2017).

There is no current consensus among groups on the most effective Vim targeting method for invasive neurosurgery (Lozano & Mahant, 2004). Surgeons typically use minimally invasive stereotactic surgery, guided by preoperative computed tomography (CT) or magnetic resonance imaging (MRI), to localize the appropriate anatomical target, usually with respect to the third ventricle, in the same plane as the anterior commissure (AC) and posterior commissure (PC). The lateral coordinate is calculated using an invisible line between the AC and the PC (known as the AC-PC line), taking into account the size of the subcortical structures established by the presurgical CT or MRI scans by correlating an atlas such as the Schaltenbrand and Wahren stereotactic atlas (Lozano & Mahant, 2004). In one particular study, the average lead placement was shown to be 12.3mm lateral to the midline, and 6.3mm anterior to the posterior commissure in the plane of the anterior and posterior commissure (Papavassiliou et al., 2004).

The electrode placement is usually further refined to optimize surgical efficacy. Microstimulations are delivered to the Vim and the VPL. Within the Vim, stimulation evokes changes in the ongoing tremor, whereas in the VPL, stimulation evokes somatic sensations and should be avoided (Garonzik, Hua, Ohara, & Lenz, 2002). Deep brain microelectrode recordings are also used to recognize specific discharge patterns from the Vim or the structures surrounding

the Vim in response to sensory stimulation, or muscle contraction and movement. In some cases, post-operative imaging may also be used to confirm the target location or to investigate complications (Lozano & Mahant, 2004; Redfern & Ruskin, 1989). The long-term failure rates for DBS placement for essential tremor are 13-40%, typically due to either physiological tolerance or suboptimal lead placements (Pahwa et al., 2006). One study looking at DBS electrode implantation in ET patients, and calculated an "optimal target" using a model of their clinical outcomes. They showed that patients whose lead locations were within 2mm of the "optimal target" on the AC-PC plane showed a much higher percentage of good tremor control post surgery (>66% improvement based on Fahn-Tolosa-Marin Tremor Rating Scale between DBS-on and DBS-off conditions), while patients with lead locations greater than 2mm from the "optimal target" were more likely to show moderate or poor tremor control (≤66% tremor improvement using the same rating scale) (Papavassiliou et al., 2004). This high amount of specificity required in DBS surgery makes the need to localize thalamic nuclei of utmost importance.

Microelectrode refinement is not an option for certain non-invasive thalamotomies such as gamma knife radiosurgery or MRgFUS. Instead, non-invasive surgeries currently rely entirely on anatomical targeting. This is a substantial drawback of radiosurgery as there is no way to verify the correct anatomical location and the appearance of the clinical effects due to surgery may take weeks or months to become evident (Frighetto, Bizzi, & Oppitz, 2011). This is less of an issue using MRgFUS as results are immediate, however, direct anatomical targeting using probabilistic atlas references is still the preferred targeting method. Some thalamic mapping is attempted using sublesional temperatures to effect changes in thalamic neuronal activity, however these mechanisms are not yet clear and remains an active area of research (Lipsman et al., 2013).

2.2 Principles of Magnetic Resonance Imaging

The need to better localize surgical targets has been illustrated in the previous section, especially during invasive surgeries such as thalamotomy and DBS. MRI is already being used for preoperative imaging to provide structural images of the patient's brain. The principles underlying this technology are important to understanding the methods used in this thesis.

2.2.1 Magnetic Resonance Imaging

MR images are formed by detecting magnetic field changes from RF stimulated protons. These protons have an intrinsic nuclear property called spin, which imparts a non-zero magnetic moment to nuclei with unpaired protons or neutrons. In the presence of an external magnetic field, protons change from a randomly oriented state to align (parallel or anti-parallel) with the direction of the magnetic field. A secondary oscillating magnetic field excites the proton. The net nuclear magnetization, which is aligned with the main magnetic field, tips from the longitudinal direction (or z-direction, aligned with the external magnetic field), towards the transverse plane (or xy plane). The net magnetization then rotates (or precesses) around the direction of the main magnetic field and then returns to the equilibrium state in the longitudinal direction. The excitation RF pulse controls the flip angle – the amount of rotation away from the z-axis that the net magnetization experiences during stimulation.

The overall magnetization evolution towards their natural equilibrium state following excitation is a process called relaxation. This is characterized primarily by two time constants: T_1, or spin-lattice relaxation time, and T_2, or spin-spin relaxation time. Following the excitation pulse, the nuclear spin regrows back towards equilibrium along the longitudinal direction of the proton's

magnetization, as seen by the green curves in Figure 2-4. The T_1 value represents the regrowth of the longitudinal signal to (1 – 1/*e*), or about 63% of its final equilibrium value.

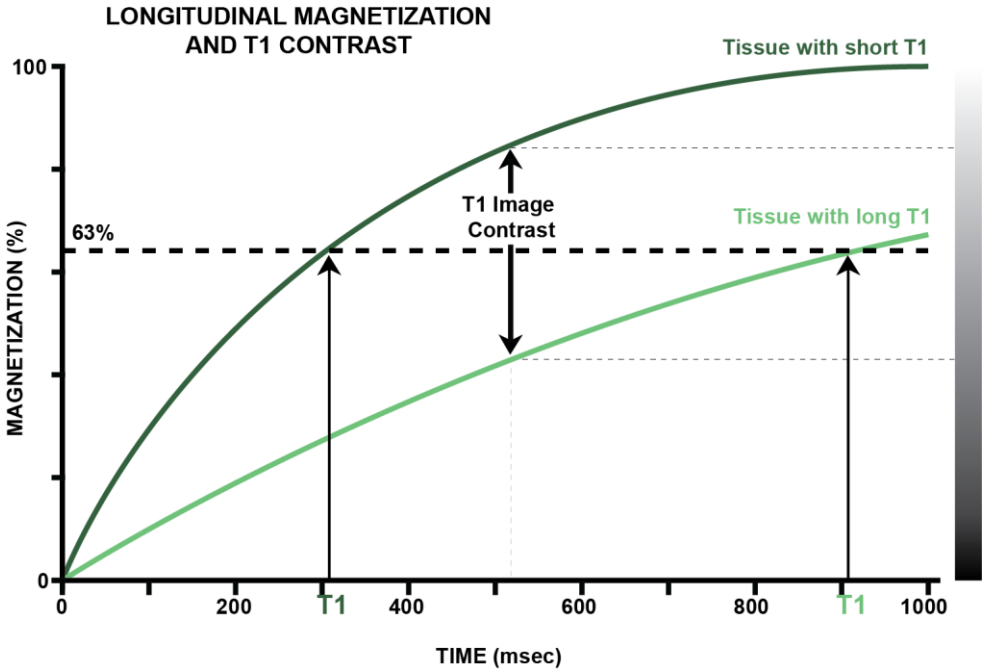

Figure 2-4: After a 90° pulse, the longitudinal magnetization recovers in the direction of the z-axis with the tissue-dependent relaxation time T_1. Tissues with shorter T_1 will appear brighter in T_1-weighted images, as shown by the contrast gradient to the right. Adapted from Sprawls, 2000.

At the same time, the transverse magnetization, seen in Figure 2-5, is at its maximum directly following the excitation pulse, and then proceeds to decrease as protons lose coherence with one another. This process of exponential decay can be characterized by the T_2 relaxation time, at 1/*e* or about 37% of the initial value following excitation. Both longitudinal and transverse magnetization components can be characterized by the solution to the Bloch equations:

$$M_z = M_0(1 - e^{-t/T1})$$

$$M_{xy} = M_0 e^{-t/T2}$$

While all images have contrast that is a mix of varied T_1 and T_2 weights, images are usually weighed towards one or the other. In the brain, T_1-weighted images produce dark cerebral spinal fluid (CSF), a grey cortex, brighter signal in the white matter, and very bright fat. T1 contrast is shown in Figure 2-4 where the dotted lines indicated tissue dependent contrast. T_2-weighted images manifest in the brain as bright CSF, light grey cortex, and darker white matter. This tissue-dependent T2 contrast can be seen in Figure 2-5.

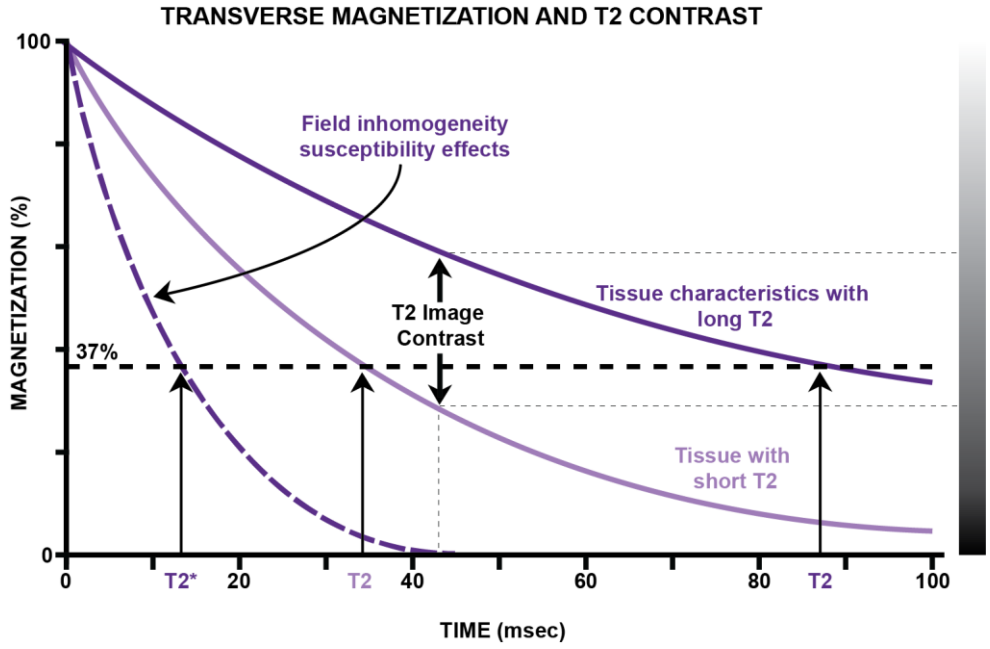

Figure 2-5: After a 90° pulse, the transverse magnetization decays with the tissue-dependent relaxation time T_2. Tissues with longer T_2 will appear brighter in T_2-weighted images. While T_2 characterizes intrinsic tissue characteristics, the presence of field inhomogeneities will shorten the decay, characterized by T_2* value, shown by the dashed purple line. Adapted from Sprawls, 2000.

Another value, called the apparent transverse relaxation time, or T_2* decay, characterizes relaxation of the observed transverse magnetization. In addition to the random atomic and molecular interactions in the intrinsic field, which cause transverse relaxation, T2* decay occurs due to additional dephasing from local field inhomogeneities and results in the shorter T2*

constant. This can be seen in Figure 2-5, where the dashed purple line depicts the T2* value, compared to the solid purple line depicting the T2 decay curve for the same tissue. These may include sources of magnetic susceptibility such as tissue iron or calcium. This has practical applications such as exploiting T_2* times to add contrast to hemorrhage, tissue calcification, or changes in blood oxygen saturation.

Besides the excitation pulse, protons are also affected by linear spatial magnetic field gradients in each of the x-, y-, and z-axes, to encode spatial information into the acquired MR signal. A slice-select gradient varies the resonance frequencies in the direction perpendicular to each slice. This ensures that only a specific width of tissue has the resonance frequency within the bandwidth of the excitation pulse. More magnetic field gradients differentiate in-plane locations; a frequency-encoding gradient is applied within each plane to vary the signals arising from different positions in one direction, while a phase-encoding gradient is similar and applied along the orthogonal direction. These gradient pulses used for this encoding are illustrated in Figure 2-6. When the MR signals are acquired, they are done so in the frequency domain, known as k-space, and image reconstruction is achieved via Fourier inversion.

The contrast between tissues is due to the relative densities of the nuclei in the tissue and the differences in intrinsic tissue properties, shown in Figures 2-4 and 2-5. Repetition time (TR), or the amount of time between successive RF pulses, is used to vary the contrast between tissues to emphasize (shorter TR) or deemphasize (longer TR) the T1 differences. Between each subsequent TR, the transverse magnetization is refocussed as a single, or many echoes. The echo time (TE) is then defined as the time from the original RF pulse to each echo. TE controls the amount of T2 relaxation – a longer TE results in more T2 weighting, while a shorter TE in less T2 weighting. The integration of TR and TE into the pulse sequence is shown in Figure 2-6.

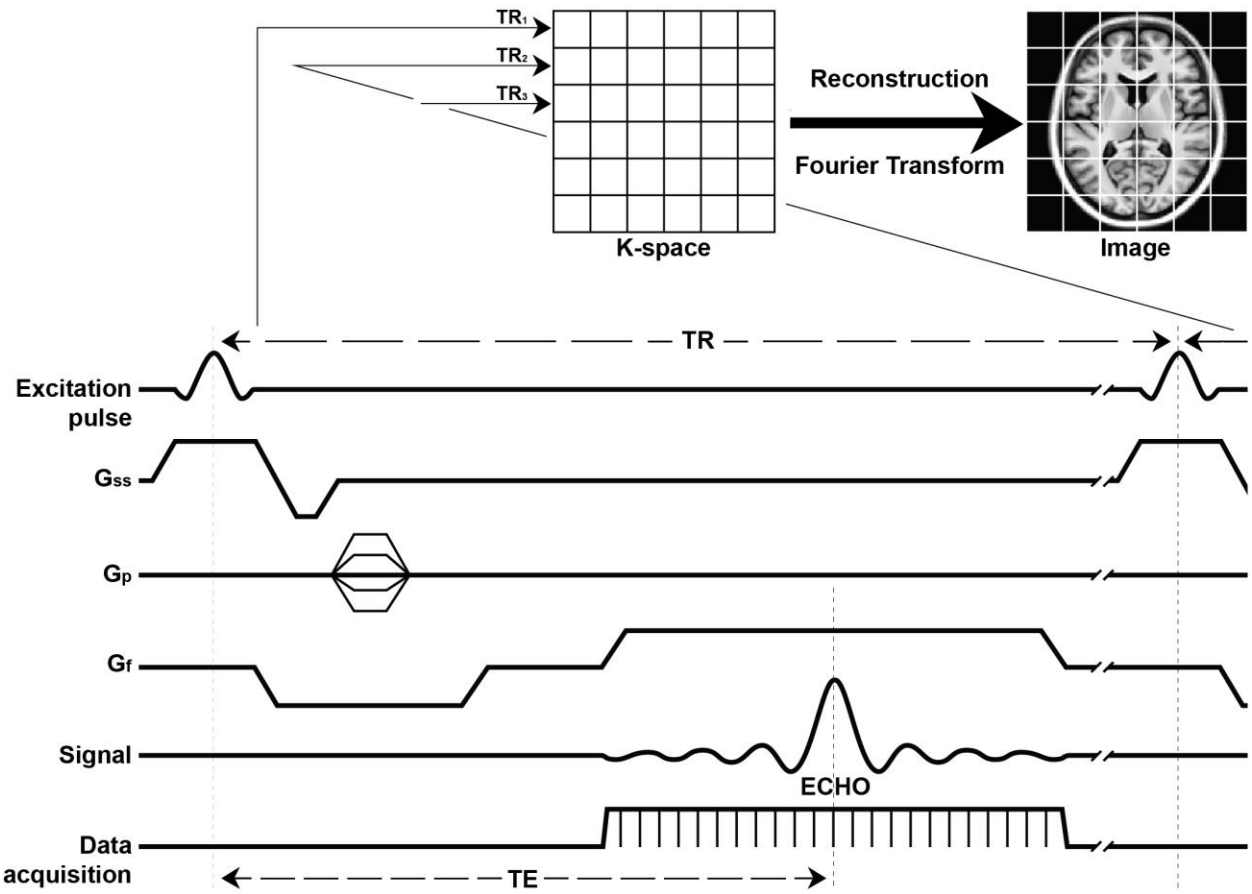

Figure 2-6: Pulse sequence diagram illustrates how images are encoded. During the excitation pulse, the slice select gradient (G_{SS}) centers the excitation pulse to a small range of the z-axis. Frequency encoding (G_f) specifies the position along the x-axis, first with a negative gradient to dephase, followed by a positive gradient to rephrase spins, focussed on the center of the acquisition window. Phase encoding (G_p) is incremented at each repetition of the pulse sequence to measure one line in k-space. K-space is then reconstructed into the image. Adapted from Buxton, 2009.

Two main MRI methods, spin echo (SE) and gradient recalled echo (GRE), exist to refocus the transverse magnetization between each TR, and these make up most of the pulse sequences used for MRI acquisition. SE use a 90° flip angle for the original excitation pulse. A 180° RF refocussing pulse, at time TE/2, is then used to remove static field inhomogeneities that cause T2* effects. GRE uses a negative frequency encoding gradient to cause some spin dephasing, followed

by a positive frequency encoding gradient of the same amplitude to cause the dephased spins to rephase. Unlike a SE, this does not remove the inhomogeneous dephasing, and results in T2* weighted images. However, the use of a GRE is also much faster as smaller flip angles can be used, resulting in less time taken for spins to regain full longitudinal magnetization, and no additional RF pulses are needed. Echo-planar imaging (EPI) uses quickly oscillating gradients to collect an entire 2D k-space in the span of a single TR, rather than a single phase-encoded line as would be typical in other MRI sequences. GRE-EPI is a fast MRI pulse sequence particularly sensitive to T2* effects. While this increases its sensitivity to susceptibility artifacts such as chemical shift, the reduced imaging time allows EPI to capture rapid physiological processes.

2.2.2 Functional Magnetic Resonance Imaging

Functional magnetic resonance imaging (fMRI) is built on the same fundamental principles as MRI but typically uses GRE-EPI to exploit the T2* effect, specifically the magnetic susceptibility properties of deoxyhemoglobin (dHb) in blood. While oxygenated hemoglobin is slightly diamagnetic, dHb is paramagnetic and creates microscopic magnetic field inhomogeneities that shorten T2* times and decrease the MR signal. Thus, there is a monotonic relationship between the oxygen saturation of blood and the T2*-weighted MR signal. This method of functional MRI is called blood-oxygen-level dependent (BOLD) imaging.

BOLD imaging allows us to indirectly look at neuronal activity levels in the brain. It is well known that changes in blood flow and blood oxygenation are coupled to neural activity. The brain does not have significant internal reserves of glucose, its primary source of energy. These resources are brought in from outside of the brain via blood flow. This is governed by a process called neurovascular coupling and can be modelled by the hemodynamic response function (HRF),

shown in Figure 2-7. When blood flow increases to transport glucose to the more active brain tissue, additional oxygen is also brought in by an increased amount of oxygenated Hb in red blood cells. This relative increase in cerebral blood flow (CBF) is larger than the relative increase in the cerebral metabolic rate of oxygen (CMRO2). As an overall result, there is a net increase in blood oxygenation, resulting in a net positive BOLD effect (Buxton, 2009).

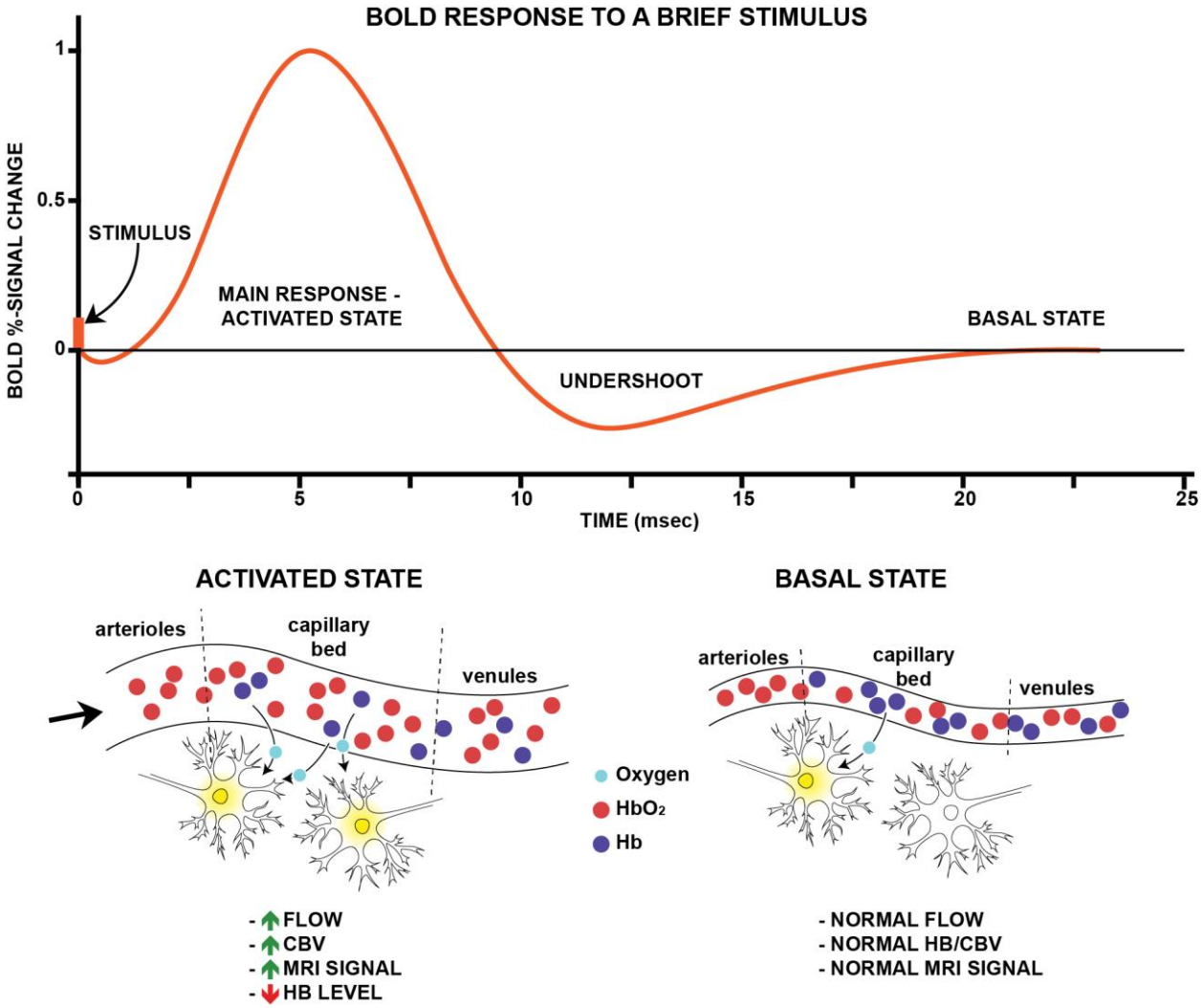

Figure 2-7: Following neural stimulus, an initial dip is seen the BOLD response because of a lag in the hemodynamic response. The main increase in the BOLD response reflects the increase in blood flow as neuronal activity continues. When the increase in blood flow is

no longer necessary, an undershoot can be seen as oxygenated blood is used up, before returning back to the basal state. Adapted from Vincent, Moore, Kennedy, & Tracey, 2009.

We can model changes in the BOLD signal using the presumed hemodynamic response function and a model of the subjects' tasks. Each individual voxel is modeled as an independent observation, and can be represented with a general linear model (GLM):

$$Y = X\beta + \varepsilon$$

The GLM as it applies to fMRI models the brain activity in each voxel (Y) as the product of the predictors, such as the stimulus task or conditions (X) and the estimated model parameters (β), plus any residuals or random error (ε). Most of the time, we're interested in the β value, which estimates the response at each voxel. Because the signal to noise ratio (SNR) in these experiments is generally poor, tasks or stimulations are repeated several times. This is commonly done in a block design, where similar events or tasks are grouped together and alternated with a baseline condition. In event-related designs, brief events or tasks occur during a sustained baseline condition. In task-based fMRI modelling, locations of significant correlated changes in BOLD signal correspond to areas of the brain activated during the execution of said task or stimulus.

In the absence of task or stimulus, there are spontaneous fluctuations in the BOLD signal. The significance of these signals was first presented by Biswal et al. in 1995 where the authors found a correlation between spontaneous fluctuations in a region in the left somatosensory cortex with the homologous areas in the contralateral hemisphere (Biswal, Yetkin, Haughton, & Hyde, 1995). The implications here were that large-scale patterns of signal could be identified across the brain in regions exhibiting functional connectivity; many networks have since been identified. These regions with correlated spontaneous fluctuations were termed "resting-state networks", and the corresponding imaging technique called resting-state fMRI (RS-fMRI).

RS-fMRI tends to exhibit higher amounts of noise due to a smaller SNR in BOLD response compared to TB-fMRI, and thus, is more susceptible to artifacts due to head motion, or other sources of noise. During signal modelling, these independently estimated noise components can be regressed out from the measured BOLD time course to improve the SNR. The analysis of RS-fMRI typically involves correlating the spontaneous BOLD fluctuations over time across the whole brain.

A seed-based analysis of RS-fMRI is the primary method used in the research outlined here. This method uses an extracted BOLD time course within a user-defined region of interest (ROI) to correlate with all other voxels in the brain. A statistical threshold is used to identify statistically significant levels of correlation. This method of analysis is a targeted approach, requiring a priori selection of an ROI or ROIs to ask a specific question of the analysis.

Another common method of analysis is independent component analysis (ICA). ICA is a mathematical decomposition technique that maximizes the statistical independence among each of the components of the whole brain signal time course. ICA can be used to identify many separate networks, as well as identify noise components of the BOLD signal. Unlike the seed-based analysis, ICA does not require a priori selection of ROI, and thus is often used for investigative analysis. While other methods of RS-fMRI analysis exist, they were not used in this study.

CHAPTER 3: **LITERATURE REVIEW**

3.1 The Need for Better Presurgical Imaging

Visualization of individual thalamic nuclei using MRI is not an easy task. On average, the Vim takes up approximately 3x8.5x5mm^3 in volume within the thalamus, which itself appears mostly homogenous when imaged using standard MRI sequences (Fang et al., 2015). In comparison, the STN and the GPi are reliably identified and can be directly visualized using current pre-operative structural MRI procedures (Vassal et al., 2012). The proximity of the VPL to the Vim also increases the difficulty of accurately targeting only the Vim for neurosurgery.

While improved MRI resolution and SNR has led to increased accuracy in subcortical targeting, the Vim itself is largely identified by neighbouring anatomical structures such as surrounding pyramidal tracts, or the internal medullary lamina (A. L. Benabid, Koudsie, Benazzouz, Le Bas, & Pollak, 2002; Morel, 2007; Yamada et al., 2010), or its location is extrapolated from the location of the AC-PC line (Redfern & Ruskin, 1989; Vassal et al., 2012). These indirect targeting methods are currently the gold standard reference for surgical targeting, however, there are many anatomical variations in deep nuclei, particularly in diseased states. For example, the location of the PC varies considerably between patients. One histological investigation revealed that the PC location, with respect to the AC, may vary up to 5.3mm in the anterior-posterior direction, and up to 6.5mm in the superior-inferior direction, and thus, suggested the use of other landmarks for thalamic localization (Redfern & Ruskin, 1989). Subject specific differences such as brain sizes and brain asymmetry are also not often taken into account (Vassal et al., 2012).

Besides anatomical differences between subjects, variability also exists amongst atlases. Atlases may be based on brains of varying sizes, ages, and number, and thus, may not necessarily

be representative of a specific patient. For example, the Chakravarty atlas is histologically defined by a single brain, while the Morel atlas is defined using six brains (Chakravarty, Bertrand, Hodge, Sadikot, & Collins, 2006; Morel, 2007). One particular study emphasized this inconsistency in atlas space by using coordinates for DBS defined by other studies, and transforming them from their native stereotactic AC/PC coordinate space into MNI space (Horn et al., 2017). They followed this up by mapping these coordinates into six different atlases. Using a target Vim as an example (Papavassiliou et al., 2004), the authors showed that the DBS targets overlaid the VPLa in the Chakravarty atlas and the VPM in the Morel atlas (Chakravarty et al., 2006; Morel, 2007), both adjacent to the Vim. In the Behrens DTI connectivity atlas (Behrens, Woolrich, et al., 2003), the DBS target lay between premotor and M1 areas in the thalamus, and in the Zhang functional connectivity atlas (Zhang et al., 2008), the target was between motor and sensory regions of the thalamus. Thus, indirect targeting is intrinsically a probabilistic method for localization. These inconsistencies highlight some of the shortcomings with the use of atlases to define small subcortical structures within a widely different population. This problem is aggravated when these targets for DBS and thalamotomies are so small. Thus, improved precision for presurgical thalamic targeting before the electrode refinement could shorten the electrophysiology refinement process in invasive surgeries and potentially improve outcome in non-invasive surgeries.

Fortunately, research to advance preoperative stereotactic imaging using MRI to determine thalamic localization has been progressing. Previous work using various MRI sequences to segment the thalamus and localize specific nuclei, including the Vim, has yielded mixed results. The primary focus of many of these sequences is to differentiate structural differences between the subnuclei of the thalamus. The cortex attenuated inversion recovery (Magnotta, Gold, Andreasen, Ehrhardt, & Yuh, 2000) and white matter attenuated inversion recovery (Vassal et al., 2012)

consistently produced plausible outlines of the ventral group of thalamic nuclei, but not with sufficient contrast detail. Inadequate image resolution and contrast remain the main confounders to producing clinically valuable pre-operative structural MRI for DBS. Development of other sequences such as the fast gray matter acquisition T1 inversion recovery (FGATIR) to image more precisely for DBS presurgical localization has also surfaced (Sudhyadhom, Haq, Foote, Okun, & Bova, 2009). While the FGATIR sequence allows for better visualization of standard DBS targets, it does not do so for specific thalamic nuclei. Rather, it focuses on localization of the entire thalamus, and other surrounding subcortical structures such as the STN and GPi.

3.2 Thalamic Nuclei Segmentation Using Structural Imaging

Diffusion tensor imaging (DTI) is a rapidly evolving approach to structural thalamic imaging, which has been used for segmentation purposes. This technique requires no contrast agents or tracers, and thus is easy to implement as part of a preoperative procedure. DTI models the diffusion of water across the architecture of the tissues, allowing researchers to view and measure the degree of anisotropy and microstructural orientation. The rate and direction of water diffusion in each voxel can be calculated, and a model for the diffusion process can be represented using a 3x3 symmetric matrix called a tensor. The tensor can be calculated from at least six diffusion encoding directions (Basser, Mattiello, & Le Bihan, 1994; Pierpaoli, Jezzard, Basser, Barnett, & Di Chiro, 1996; Soares, Marques, Alves, & Sousa, 2013). In the brain, DTI is typically used to view white matter fibre tracts that connect cortical and subcortical regions, as well as local networks. Because of the high information content from the number of directions generated, DTI is highly sensitive to pathology in the brain, and may also be used to look at subtle changes in specific white matter tracts.

An early study showed that the white matter tracts which ran up from the thalamus could be mapped to the cortex using DTI and probabilistic tractography (Behrens, Johansen-Berg, et al., 2003). With respect to the motor and sensory areas, Behrens et al. traced individual thalamic voxels within the ventral lateral nucleus to the motor cortex, meeting the expectations based on anatomy literature. The same group followed up this study by comparing the DTI tractography to cytoarchitecture and functional imaging found in literature to further validate their thalamic parcellation (Johansen-Berg et al., 2005). In both studies, probabilistic representations were used to determine overlapping cortical connections. The authors also showed a wide variation in thalamic nuclei location, based on varying diffusivity rates and directions. Based on this research, the use of DTI to look at thalamic nuclei using their white matter cortical connections became more popular. Using this methodology, a proof-of-concept trial was carried out using healthy controls to define the Vim and the Vop using their respective thalamocortical connections to M1 and the premotor cortex. The results showed large inter-subject variability in the estimated Vim and Vop location, with the mean pair-wise inter-subject distance ranging over 14mm for both the Vim and the Vop. This was followed up by two thalamotomy case studies where this DTI-based method was used for pre-surgical targeting. In these two cases, both the Vop and the Vim were used as thalamotomy targets, and were successfully targeted (Kincses et al., 2012).

Many algorithmic approaches to categorizing DTI results have also been used to do this with some success. Wiegell et al. showed it would be possible to resolve the major nuclei solely based on fiber orientation of corticothalamic tracts using a clustering algorithm (Wiegell, Tuch, Larsson, & Wedeen, 2003). This clustering algorithm was set to 14 clusters based on visual inspection of original renderings, of which 8 were determined to be within the bounds of the assigned anatomical nuclei when compared with Morel's stereotactic atlas. While 8 clusters does

not have a high enough specificity to determine the exact location of the Vim, six of these clusters did show correlation with the Niemann histology atlas, including the VPLa. The Vo was significantly different than the expected location when compared to the histological atlas. Thus, the complexity of subnuclei within the thalamus may prevent DTI from being able to reliability identify the Vim further. A similar recent study automated the segmentation of the thalamus using multi-modal features such as tissue contrasts from T1-weighted, as well as fractional anisotropy, fiber orientation, and principal eigenvectors from diffusion weighted images (Stough et al., 2014). While their automated parcellation resulted in regions quite similar to manual delineation, they were also not specific enough to parcellate individual ventral thalamic nuclei.

Research has also been conducted looking at the connections between the thalamus and other subcortical counterparts, particularly the basal ganglia (Lenglet et al., 2012). Other studies used these approaches to thalamic parcellation to conduct more detailed research to identify the thalamic nuclei involved in motor function and dysfunction. Hyam et al., specified thalamic seeds within the Vim and Vop to evaluate connectivity through the thalamus. Using DTI, they traced the white matter tracts starting from the Vim to the cerebellum, and M1, and from the Vop to the SMA and the dorsolateral prefrontal cortex. These results are also well-supported by cytoarchitecture found in non-human primate histological studies (Hyam et al., 2012). Newer studies have used more diffusion encoding directions, higher resolution, and longer acquisition times to investigate these pathways in tremor patients. Akram et al., showed that DBS response was most effective when the DBS leads connected to the thalamic area exhibiting the highest connectivity to the contralateral dentate nucleus within the dentate-rubro-thalamic (DRT) tract (Akram et al., 2018). This particular tract, seen in Figure 3-1 starts at the dentate nuclei, ascends through the fourth ventricle and relays through the red nucleus. While some fibers terminate here, the majority

continue through to the thalamus and terminate within the Vim and the Vop, located adjacent to the Vim (Coenen, Allert, & Mädler, 2011).

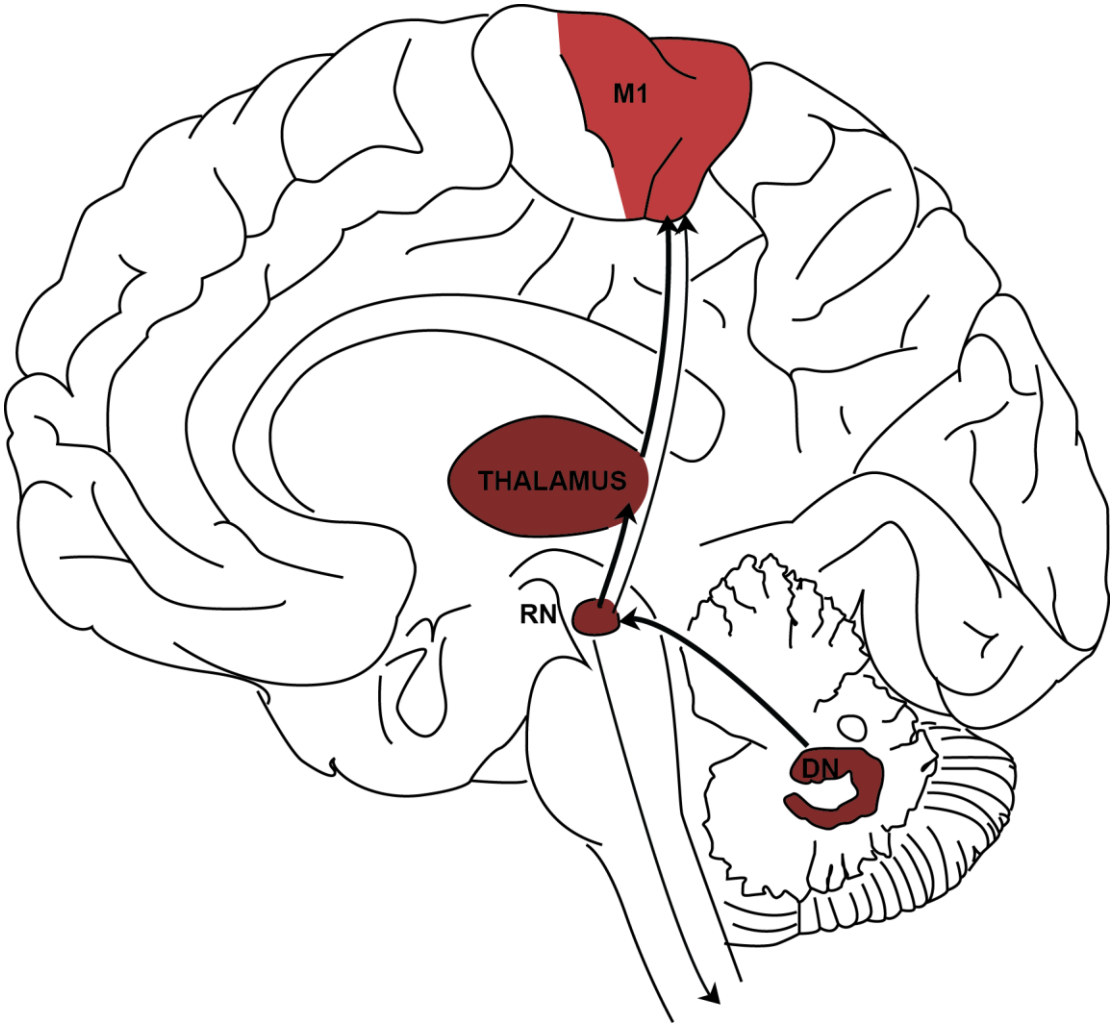

Figure 3-1: The DRT is shown schematically in the bolded line. Adapted from Guyton & Hall, 2006.

Other studies use DTI to localise surrounding structures as landmarks to locate the Vim. Yamada et al., overlaid structural diffusion images with T1-weighted anatomical images and traced cortical tracts using ROIs placed at the red nucleus and white matter adjacent to the primary motor cortex. They were able to identify the Vim and VPL using the surrounding pyramidal tracts, the internal medullary lamina, and other thalamic nuclei in healthy subjects (Yamada et al., 2010).

A similar study was done on a patient cohort by Sammartino et al., where the Vim borders were defined by surrounding pyramidal tracts and the medullary lamina. Tractography results were found to be a little over 10mm farther anterior and lateral as compared to the conventional microelectrode targeting method, however, this area correlated with electrophysiological results. Further tractography from the Vim target was investigated, however this was not successful in all subjects. In those whose Vim projections were trackable, the DRT was found to be among the more prominent tracts. Cortical projections to M1 were also consistently found in almost all subjects (96% of hemispheres in ET patients, 100% of hemispheres in controls) while projections to the premotor cortex were only found in few subjects (7.7% of hemispheres in ET subjects, 13.8% of hemispheres in Controls) (Sammartino et al., 2016).

Contrary to these findings, a different study showed that the DBS-stimulated area in the thalamus exhibits much higher connectivity with the premotor cortex compared to M1 in patients who had already undergone DBS implantation surgery (Pouratian et al., 2011). Pouratian et al., advised the future use of premotor and supplementary motor area tracts to target the Vim. While few studies have actually integrated DTI as part of the presurgical routine, Coenen et al., presented a case study investigating the plausibility of this in a single subject. In the reported case study, the group targeted the DRT within the thalamus, and used the resulting area as the DBS target. This lead to a successful DBS implantation and tremor alleviation. The DRT runs through the Vim, but also through the posterior STN and caudal zona incerta (cZI), both of which have been researched alternate targets for tremor alleviation (Coenen et al., 2011).

3.3 Thalamic Nuclei Segmentation Using Functional Imaging

Functional imaging is yet another method used to localize specific thalamic nuclei, which also has mixed results. Positron emission tomography (PET) was first used for functional brain imaging. The technique uses a radionuclide tracer which undergoes positron emission decay as it travels through the blood circulation in the brain. The PET scanner detects the changes in radioactivity as the tracer moves, and 3D or 4D images are made to observe metabolic and hemodynamic processes. Most of the functional imaging studies used $H_2{}^{15}O$ as the tracer to gauge regional alterations in cerebral blood flow (Ceballos-Baumann, 2003). Early PET studies were used to identify changes in cortical activation following a thalamotomy in tremor-dominant PD (Boecker & Brooks, 1998; Boecker et al., 1997).

More recent studies have also suggested that functional MRI (fMRI) can localize the Vim or the VPL with accuracy (Anderson et al., 2011; Ghaderi, Sadikot, & Pike, 2014). In comparison to PET, fMRI has higher spatial resolution, is safer (no ionizing radiation), and is non-invasive (no injections). Few studies have used fMRI as a method specifically for presurgical thalamic targeting, however, resting-state methods have been used for thalamus segmentation.

Many groups have used known thalamocortical connectivity to parcellate the thalamus. Fan et al., used a K-means clustering algorithm on resting-state functional connectivity profiles of the thalamus to determine the optimal number of clusters. This value was assessed using variation of information and Dice's coefficient and a value of K=7 was selected. Of these, only two were highly connected to the motor network, however, not with the expected specificity based on known Vim size (Fan et al., 2015). Similarly, a spectral clustering algorithm has also been used to generate connectivity matrices for thalamic parcellation, using an atlas to define the finer thalamic structures (Ji et al., 2016).

Whole brain functional networks have also been used to segment the thalamus based on thalamocortical connectivity. Five large cortical seeds representing the prefrontal, parietal/occipital, motor/premotor, somatosensory, and temporal cortical areas were used to segment the thalamus using seed-based partial correlation, and the results compared to white matter tracts from the same cortical seeds to their structural thalamic counterparts (Zhang, Snyder, Shimony, Fox, & Raichle, 2010). The same cortical areas have also been used for seed-based analysis, and compared to thalamic segmentation using ICA to compare thalamocortical network patterns using different RS-fMRI analysis methods (Hale et al., 2015). While neither of these studies parcellated the thalamus with clinical use in mind, they open the field for the potential use of seed-based connectivity for thalamic presurgical mapping. Anderson et al. attempted to identify the Vim using RS-fMRI connectivity from a functionally defined (using a 4-min finger tapping task), combined, primary motor cortex and cerebellar seed. They found the resulting thalamic connectivity in healthy subjects within 5mm of the thalamic DBS location, specified by their neurosurgeon (Anderson et al., 2011).

CHAPTER 4: **HYPOTHESIS**

We hypothesize that RS-fMRI can be used as a preoperative imaging procedure to achieve preliminary localization of the Vim and VPL. Characterizing the accuracy and specificity of RS-fMRI will allow us to optimize pre-operative surgical planning procedures and shorten surgical time for ET and tremor-dominant PD patients undergoing thalamotomy. In the future, these localization methods could be modified for direct thalamic targeting in non-invasive surgeries where electrophysiological refinement can not be used. To test this hypothesis, we have two goals.

The first goal is confirmation that task-based fMRI (TB-fMRI) can reliably localize the motor and somatosensory areas of the thalamus. Following this, the second goal is to determine if the thalamic motor region localized using TB-fMRI can be replicated using RS-fMRI. The advantages of RS-fMRI would be the ease of use for presurgical planning.

The feasibility of using fMRI as a method for presurgical imaging for thalamic surgery not only depends on the precision of localization within the thalamus, but also on the ability to replicate localization results in diseased states. Thus, another goal is to compare the strength of thalamic activation in TB-fMRI and the strength of connectivity in RS-fMRI to determine the feasibility of using these techniques for Vim localization in PD and ET patients.

CHAPTER 5: **METHODS**

5.1 Participant Selection and Image Acquisition

All data were collected at the Montreal Neurological Institute between 2010 and 2017. Subjects were categorized into ET and PD patient groups, and healthy controls (Table 5-1). The cohort included: 21 presurgical PD patients (15M, 6F; mean age of 61.7 ± 7.3), 7 postsurgical PD patients (7M, 0F; mean age of 60.1 ± 7.5), 8 presurgical ET patients (6M, 2F; mean age of 68.1 ± 7.0), 6 postsurgical ET patients (3M, 3F; mean age – 72.3 ± 11.0) and 32 healthy controls (17M,15F; mean age – 59.8 ± 9.4). 3 PD and 3 ET patients have both presurgical and postsurgical scans. Several presurgical patients are awaiting surgery, while some postsurgical patients were not involved in this study until after their surgery. The ET and PD groups were pre-screened using the Unified Parkinson's Disease Rating Scale (UPDRS) (Goetz et al., 2007) and Tremor Score (Fahn, Tolosa, & Marín, 1988), by a neurologist, prior to participation in this study. Healthy participants were screened for normal cognitive function using the Mini Mental State Examination (MMSE) (Folstein, Folstein, & McHugh, 1975), requiring a score of 30/30. All experiments were performed with the subjects provided informed consent.

Subject Group	Protocol	# of Subjects	Sex	Mean Age ± SD
Controls	Vibrotactile Task	29	16M / 13F	58.8±7.8
	Motor Task	25	13M / 12F	57.7±9.4
	Resting State	23	12M / 11F	58.7±6.8
	Total	32	17M / 15F	59.8±9.4
Presurgical Parkinson's Disease	Vibrotactile Task	19	13M / 6F	61.7±7.4
	Motor Task	17	12M / 5F	63.5±6.2
	Resting State	13	10M / 3F	63.2±6.6
	Total	21	15M / 6F	61.7±7.3
Postsurgical Parkinson's Disease	Vibrotactile Task	7	7M	60.1±7.5
	Motor Task	7	7M	60.1±7.5
	Resting State	5	5M	58.6±8.1

	Total	7	7M	60.1±7.5
Presurgical Essential Tremor	Vibrotactile Task	7	6M / 1F	70.4±2.8
	Motor Task	5	4M / 1F	67.6±9.1
	Resting State	3	2M / 1F	71.3±2.3
	Total	8	6M / 2F	68.1±7.0
Postsurgical Essential Tremor	Vibrotactile Task	6	3M / 3F	72.3±11.0
	Motor Task	5	3M / 2F	69.8±10.2
	Resting State	3	1M / 2F	70.0±14.2
	Total	6	3M / 3 F	72.3±11.0

Table 5-1: Summary of subjects in each group. Due to changes in protocol over time and ability of the subjects to carry out various tasks, a varying number of patients was used for each task and resting state analysis. For example, 29 out of 32 subjects completed the vibrotactile task, while only 23 of them completed the resting state scan.

Multimodal datasets were collected from each patient using a 3T Siemens TIM Trio with a 32-channel head coil. T_1-weighted (T1w) anatomical, diffusion, magnetization transfer, TB-fMRI and RS-fMRI data were collected. In this study, the T1w anatomical images, TB- and RS-fMRI data will be used. Full head T1w scans were acquired at 1-mm isotropic resolution using a 3D-MPRAGE sequence, TR/TE/flip of = 2300ms/2.98ms/9°. Both TB- and RS-fMRI scans were collected using a 4-mm isotropic voxel resolution, multi-slice EPI, and TR/TE/flip = 3000ms/30ms/90°. Two TB-fMRI paradigms were selected to activate motor and sensorimotor areas. A simple motor task, where participants were asked to tap alternating fingers at a constant pace, was used to examine activation of the motor network. The pace was cued with an auditory stimulus at 90 beats per minute. A sensory task-based experiment was then conducted using a custom vibrotactile stimulator (Chakravarty, Broadbent, Rosa-Neto, Lambert, & Collins, 2009) on the right hand to activate somatosensory pathways. Both motor and vibrotactile tasks were designed with an epoch of 15s-on, 15s-off block design for a total of 2 runs of 6 min per task. Resting state scans were 6 min long and acquired with the subjects' eyes closed.

5.2 Data Processing

Images were preprocessed using the FSL software package (Analysis Group, FMRIB, Oxford UK) (Smith et al., 2004). T1w anatomical images were reoriented to standard MNI orientation, registered to standard space (MNI 2mm brain template) using linear registration (using FMRIB's Linear Image Registration Tool – FLIRT) followed by non-linear registration (using FMRIB's Non-linear Image Registration Tool – FNIRT). Following this, brain extraction was performed using the brain extraction tool (BET), and tissue-type segmentation was performed using FMRIB's Automated Segmentation Tool (FAST), separating the brain into the white matter, grey matter, and cerebral spinal fluid (CSF) components. FMRI data underwent similar standard preprocessing, including high-pass temporal filtering, motion correction, interleaved slice-timing correction, brain extraction, and linear and non-linear registration to the T1w structural image and to standard space, respectively. All preprocessing was performed using the FEAT tool. Due to the small size of the target nuclei, no spatial smoothing of the functional data was performed to avoid further reducing the spatial resolution. Additional preprocessing was performed on RS-fMRI scans to remove nuisance regressors, controlling for changes in BOLD fluctuations due to motion, cardiac and respiratory cycles. Automatic independent component analysis (ICA)-based artifact removal was done using FSL-AROMA to specifically remove movement-related components (Pruim et al., 2015). Time course signals from white matter and ventricle regions were extracted using tissue type segmentations from T1w images as masks, and head motion parameters were acquired from the previous MCFLIRT output (motion correction tool within FEAT). These signals were regressed from the time course and the residuals were used for further analysis.

For this study, a seed-based correlation was used for the RS-fMRI analysis to isolate the motor and somatosensory thalamocortical networks. Seed choice was defined based on grey matter

segmentations in the Juelich Histological Atlas (Figure 5-1). Previous studies have indicated that the Vim is functionally connected to the primary motor network (Anderson et al., 2011; Fang et al., 2015; Hyam et al., 2012; Kincses et al., 2012). Thus, to isolate the motor network, Brodmann area 4 (BA4), located posterior to the precentral sulcus and anterior to the central sulcus, associated with the M1 was chosen for the ROI. Specifically, the postero-medial portion of BA4 approximately corresponded to hand and finger representation within the motor homunculus, defined by visual inspection using the hand knob (Yousry et al., 1997), was used. Similarly, Brodmann area 3 (BA3), located posterior to BA4 between the central sulcus and the postcentral sulcus, which is associated with the primary somatosensory cortex (S1) was chosen to isolate the somatosensory network. Brodmann area 3 can be subdivided into BA3a and BA3b. The ROI used was BA3b, which isolated the hand and finger representational area within the sensory homunculus, located medially within S1, adjacent to the motor hand and finger representative areas. Both ROIs were thresholded to a 50% probability, leaving ROI sizes of 2576mm^3 for the BA3 seed and 1776mm^3 for the BA4 seed, both defined in MNI space. These ROIs were further masked by their intersection with individual anatomical grey matter segmentations to avoid sampling the time course in the white matter.

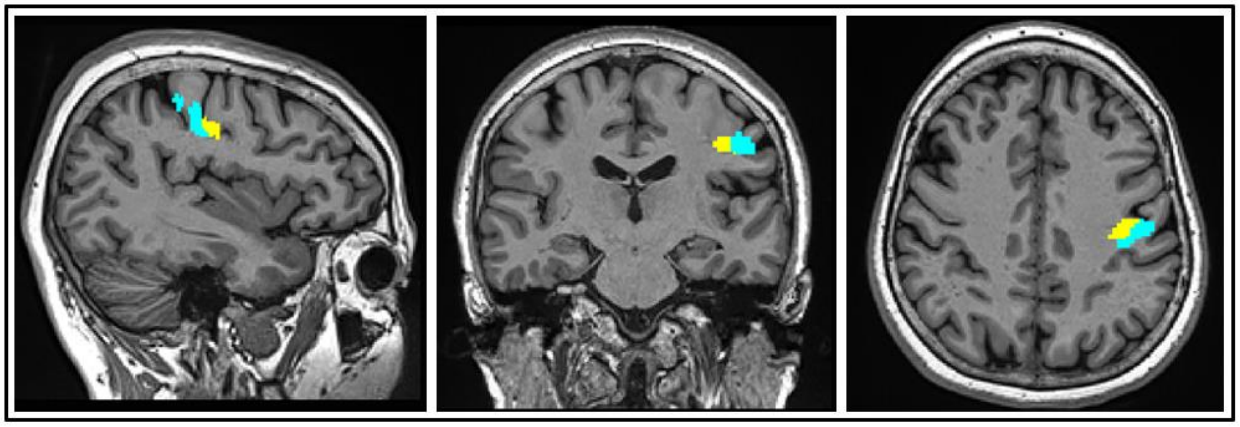

Figure 5-1: Full seed ROI based on Brodmann's Areas. The yellow seed ROI is within the posterior region of Brodmann's Area 4 associated with M1. The cyan seed ROI is within Brodmann's area 3b, associated with S1. Both seed ROIs are shown transformed into an individual subject space and have not been masked by individual grey matter segmentation.

5.3 Subject-level fMRI Analysis

After preprocessing, analysis for the motor and vibrotactile TB-fMRI runs was carried out using a GLM, the default data model within the FEAT tool. Each run was analyzed using a double-gamma HRF. Time-series statistical analysis was carried out using FILM (FMRIB's Improved Linear Model) with local autocorrelation correction and runs for each subject were combined using fixed effects higher-level modelling (Woolrich, Ripley, Brady, & Smith, 2001). Vibrotactile tasks and motor tasks were then analyzed separately.

For resting state analysis, the preprocessed residual time series was normalized by subtracting the mean and dividing by the standard deviation. The average time course for all voxels within each ROI was extracted. Regression analysis was performed using the normalized residual volume data and the extracted seed time course for each participant. This produced subject-level correlation maps of all voxels that positively correlated with the seed area. Unthresholded single

subject contrast of parameter estimate (COPE) files were inputs for group-level analysis for all fMRI runs.

5.4 Group-level fMRI Analysis

Group-level analysis for both TB- and RS-fMRI were obtained using FSL-FLAME (FMRIB's Local Analysis of Mixed Effects) methods for modelling inter-subject variance. A single group average was obtained by running a one-sample t-test separately for each group. Both individual and group results were controlled for multiple comparisons using false discovery rate (FDR) set at $p = 0.05$ using a whole brain mask. Z-statistic maps were then produced to show which voxels were significantly activated by the vibrotactile or motor task. A thalamic mask derived from the combined premotor, motor and somatosensory thalamic areas based on the DTI connectivity atlas (Behrens, Woolrich, et al., 2003) was used to isolate the relevant activation in the thalamus. Coordinates of the peak voxel in each group was used to compare to Vim-DBS locations found in the literature, and to lesion locations in the postsurgical subjects. Maximum z-statistic values were obtained to compare the strength of thalamocortical activation between groups.

5.5 Thalamotomy Location

Thalamotomy lesions visible on post-surgical subjects were traced out manually on T1w scans within FSLview. All subject lesions (from both PD and ET patients) were transformed into standard MNI space and combined to form a heat map. The voxel of highest intensity within the heat map was used as the lesion location and compared with group and single subject motor and

sensory thalamus regions localized with TB- and RS-fMRI and Vim and VPL locations from the literature.

5.6 Third Ventricle Volumetric Analysis

The size of surrounding structures may be a confound to the Vim location due to changes in the brain in pathological states. It has been frequently noted that the third ventricle may be enlarged in subjects with various conditions including schizophrenia and other psychiatric patients (Bornstein, Schwarzkopf, Olson, & Nasrallah, 1992; DeMeyer et al., 1984), multiple sclerosis (Müller et al., 2013), and Alzheimer type dementia progression (Luxenberg, Haxby, Creasy, Sundaram, & Rapoport, 1987). A few studies have reported third ventricle size in patients with movement disorders, citing an increase in patients with movement disorders (Nelson, Andy, & Foshee, 1964). Studies have also reported age-dependent increases in third ventricle size (Haug, 1978), while others have found no difference between age, sex or specific movement disorder (A. Benabid et al., 1996; Nelson et al., 1964). Third ventricle volumetric analysis was therefore added to the analysis post-hoc to account for potential differences in Vim localization between subject groups.

The default MNI 2mm standard brain was segmented using FreeSurfer (Fischl, 2012). The subsequent third ventricle mask was transformed to individual subject anatomical images (Figure 5-2). This mask was used to isolate the third ventricle in each subject using the CSF component of the segmented structural T1w anatomical scan. The total volume, x-, y-, and z-direction measurements of the third ventricle was obtained for each subject. An ANCOVA (Analysis of Covariance) using the dimensions of the third ventricle was used to evaluate whether third ventricle size affected Vim localization.

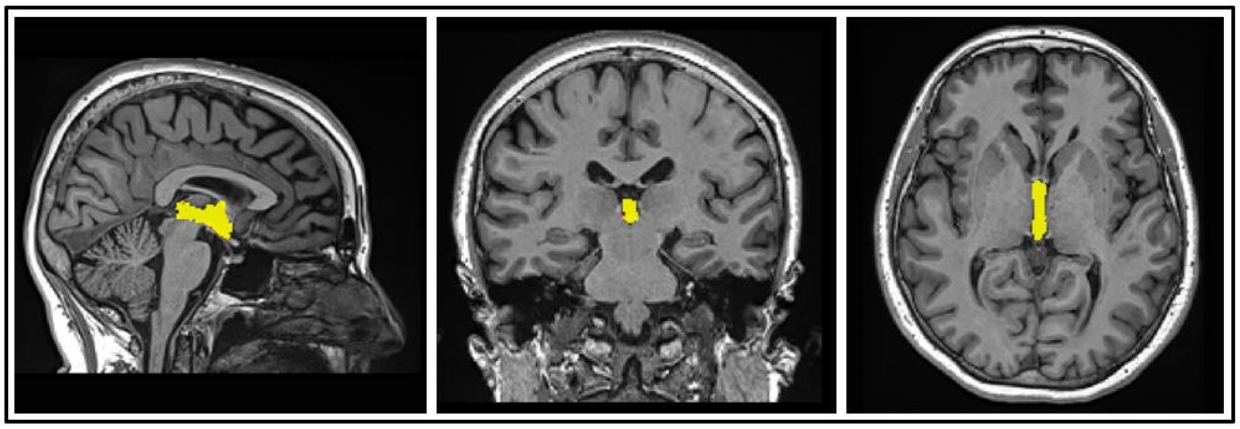

Figure 5-2: Third ventricle mask transformed from standard 2mm MNI space to a single subject T1w anatomical image.

5.7 Individual Subject Statistics

The thalamic mask derived from DTI data was also used to obtain the individual peak thalamic connectivity location coordinates and strength of connectivity measured using the z-statistic within the voxel. The coordinates, defined in MNI space, were used to calculate distances to the group mean, masked lesion location from the post-surgical subject pool and two literature-defined average lesion locations (Anderson et al., 2011; Papavassiliou et al., 2004). These coordinates were also plotted in 2D scatterplots to visualize the spread of parcellated motor and sensory thalamus locations using R (R Core Team, 2013). Further statistics was carried out using SPSS (IBM SPSS Statistics for Windows, Version 24.0. Armonk, NY: IBM Corp). The Shapiro-Wilk test for normality and Levene's test for homogeneity of variance were used for all comparisons. If the data was normality distributed and exhibited homogeneity of variance, a one-way analysis of variance (ANOVA) test was used to test for differences between groups. Significance found using the one-way ANOVA was further examined using a Student's t-test. When necessary, a nonparametric test of the null hypothesis, the Kruskal-Wallis one-way analysis

of variance test, was used instead of a one-way ANOVA. Significance found using the Kruskal-Wallis test was then examined using the Mann-Whitney U test to compare two groups. The significance level was defined as $p < 0.05$ after all tests.

CHAPTER 6: **RESULTS**

6.1 Post-Surgical Lesion – Vim localization

From our post-surgical subject pool, the combined PD and ET left lesion site was located at MNI coordinates x = -16, y = -12, z = 4, as seen in Figure 6-1. This distance, summarized in Table 6-1, measured 11.0mm from the defined Vim location referenced in Anderson et al., and 9.2mm from the average Vim location from Papavassiliou et al (Anderson et al., 2011; Papavassiliou et al., 2004). Distances from the center of mass were also compared to literature peak and were found to be closer to literature Vim points. However, the peak voxel will be used for further comparisons because it may be more representative of the whole post-surgical sample size considering the relatively small number of post-surgical subjects. Compared to both of the literature defined Vim locations, our targeted Vim location was further anterior, and slightly more lateral and superior

.

Subject Group		Coordinates (MNI space) x	y	z	Distance to Literature Peak[1]	Distance to Literature Peak[2]
Lesion	Peak Voxel	-16	-12	4	11.0mm	9.2mm
	Center of Mass	-13.19	-12.94	4.27	9.7mm	8.3mm
Literature Peak[1]		-12.5	-22	1	---	4.7mm
Literature Peak[2]		-13.05	-18.38	-2.01	4.7mm	---

[1] Anderson et al., 2011
[2] Papavassiliou et al., 2004

Table 6-1: Both peak voxel and center of mass locations are acquired from the heatmap. All distances were calculated using Euclidean distance.

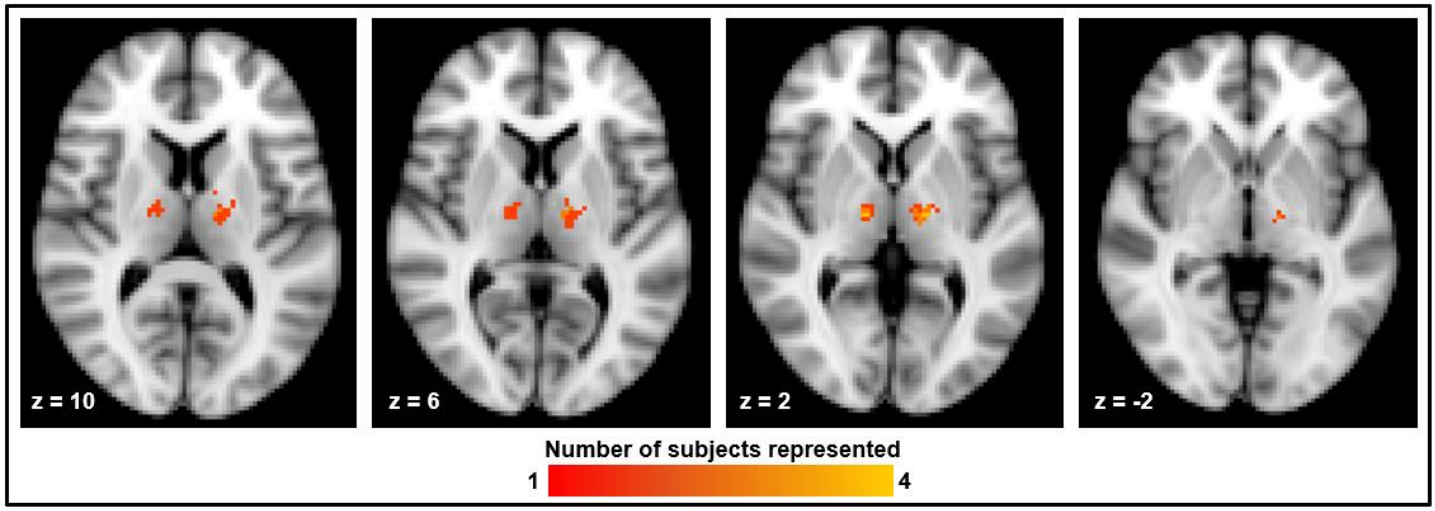

Figure 6-1: The combined lesion heat map created by adding together all postsurgical subject lesions. A total of 12 subjects were included in this heat map, six PD patients and six ET patients. Of these, 8 have left thalamic lesions (3 PD), and 4 have right thalamic lesions (3 PD).

6.2 Localization using Task-Based FMRI

Regions activated in group correlation following the motor and somatosensory tasks showed a close proximity to the expected Vim and VPL location. Robust thalamocortical connectivity was seen in the Controls, with the thalamus showing a significant volume of activation. The peak voxels were x = -16, y = -20, z = 10 for motor thalamus localization, and x = -16, y = -22, z = 0 for sensory thalamus localization. These coordinates are inline with expected Vim and VPL locations relative to one another, with the Vim further anterior.

Pre-surgical ET group correlations localized the motor thalamus (Figure 6-2B) at x = -16, y =-20, z = 0, although, FDR-corrected somatosensory group task maps in the ET group showed no significant activation within the thalamus. Unthresholded somatosensory ET maps show the peak thalamic activation at x = -16, y = -20, z = 2, however not reaching the level of statistical

significance. To provide an idea of TB-fMRI localization potential the thresholds were lowered for Figure 6-2B to visualize the activation in the thalamus. As a result, the TB-fMRI data in Figure 6-2B is thresholded at $p = 0.15$ (green, overlapping the motor thalamus activation) for visualization purposes only. The inability to find statistically significant sensory thalamic activation in this group may have implications regarding changes in thalamic function, and the validity of using TB-fMRI within the ET subject group.

The localized motor and sensory thalamus regions in the pre-surgical PD group were close to the Control group's motor thalamus location, at x = -12, y = -16, z = 10 and the sensory thalamus location at x = -18, y = -22, z = 2 (Figure 6-2C). Similar to the Controls, these coordinates are also in line with the expected relative anatomical locations of the Vim and VPL. The volume of activation remaining following statistical corrections was not as robust as those in the Control group. As a result, the localized motor and sensory thalamus appear more distinctly separated using TB-fMRI, with a smaller volume of overlap between them.

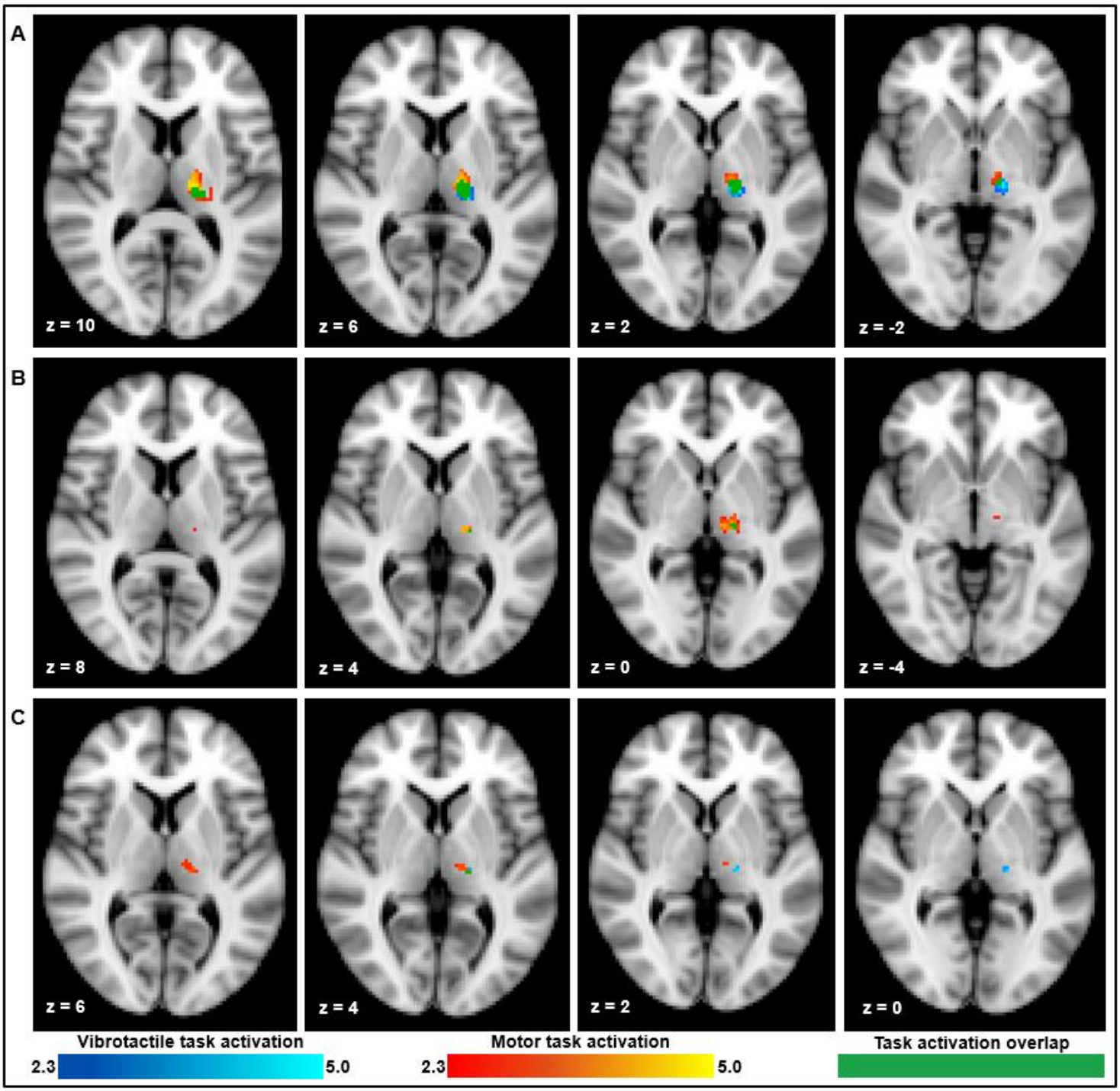

Figure 6-2: A) Control group thalamic activation. Thresholded with FDR at p = 0.05. B) Essential tremor group thalamic activation. Motor task activation is thresholded to p = 0.05 with no multiple comparisons and vibrotactile task activation is thresholded at p = 0.15 for display purposes only. C) Parkinson's Disease group thalamic activation. Thresholded with FDR at p = 0.05.

A comparison of each of these three groups' parcellated motor thalamus locations, summarized in Table 6-2, shows that the PD group is the closest, by a small margin at 8.2mm, to the lesion site in the heat map. Compared to literature defined Vim locations, the Control and PD groups have motor thalamus localizations farther superior, measuring 9.9mm and 10.8mm away from the Vim defined by Anderson et al. (Anderson et al., 2011), and 12.5mm and 12.3mm from the work by Papavassiliou et al., (Papavassiliou et al., 2004). The motor thalamus defined within the ET group is <5mm from both literature defined Vim locations (4.2mm and 3.9mm), and thus, serves as a convincing localization, but noting the limited thalamic activation. The coordinates shown in Figure 6-3 compare heat map defined lesion coordinates, to the motor thalamus localizations in the Control, PD and ET groups, at the same horizontal slice.

Subject Group		Coordinates (MNI)			Distance to Lesion	Distance to Literature Peak[1]	Distance to Literature Peak[2]
		x	y	z			
Controls	**motor**	-16	-20	10	10mm	9.9mm	12.5mm
	sensory	-16	-22	0	---	---	---
Parkinson's Disease	**motor**	-16	-20	0	8.2mm	10.8mm	12.3mm
	sensory	-16	-20	2	---	---	---
Essential Tremor	**motor**	-12	-16	10	8.9mm	4.2mm	3.9mm
	sensory	-18	-22	2	---	---	---

[1] Anderson et al., 2011
[2] Papavassiliou et al., 2004

Table 6-2: Summary of coordinates and distances from each subject group to each of the landmark points for this study following TB-fMRI localization results.

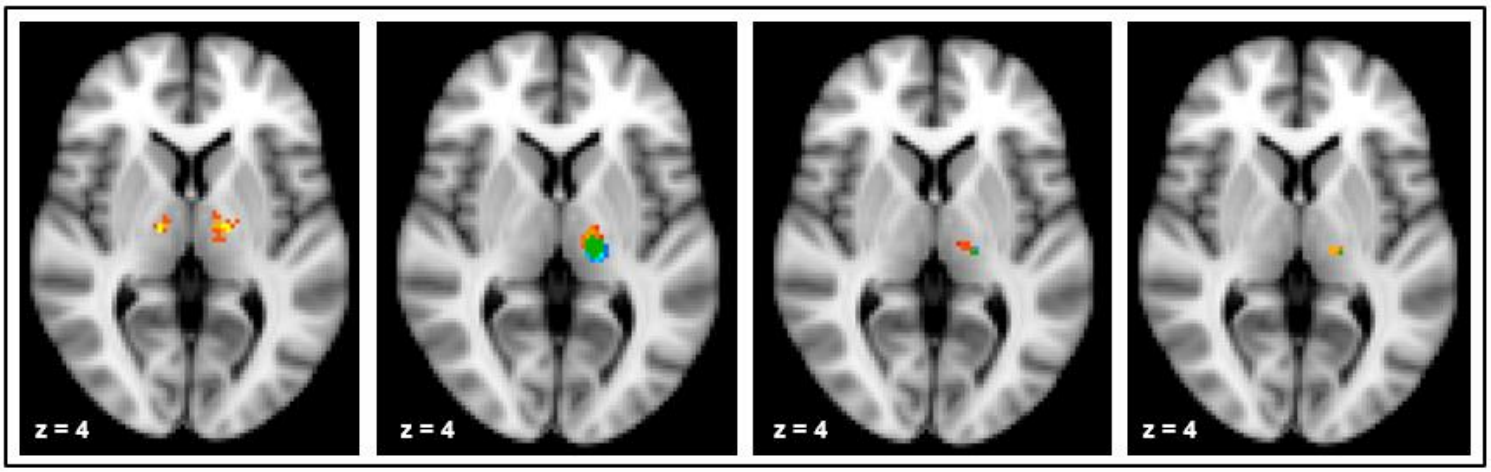

Figure 6-3: Comparison of Vim location to the lesion at slice z = 4, left to right – lesion heat map, Controls, ET, and PD.

6.3 Localization using Resting-State FMRI

A limited number of ET subjects had RS-fMRI runs (presurgical n = 3, postsurgical n = 3), and therefore the ET group was not included in the resting-state analysis.

The Control group showed robust RS-fMRI thalamocortical correlation within the thalamus, similar to the activation results obtained using TB-fMRI (Figure 6-4A). The motor and sensory thalamus peaks found using RS-fMRI correlated reasonably to the anatomical Vim and VPL positions based on previous histological studies. The peak voxels for the parcellated motor thalamus at x = -10, y = -22, z = -4, and sensory thalamus at x = -14, y = -28, z = -4 are noticeably inferior when compared to TB-fMRI motor and sensory thalamus locations, the lesion heat map, and the literature Vim locations. The RS-fMRI parcellations are also more posterior and more lateral.

The PD group RS-fMRI motor and sensory thalamus localization results were located inferiorly when compared to TB-fMRI parcellations equivalents (Figure 6-4B), similar to the RS-

fMRI parcellations in the Control group. Similar to the TB-fMRI parcellation, the thalamic correlation in the PD group was less robust than within the resting-state Control group thalamic parcellation.

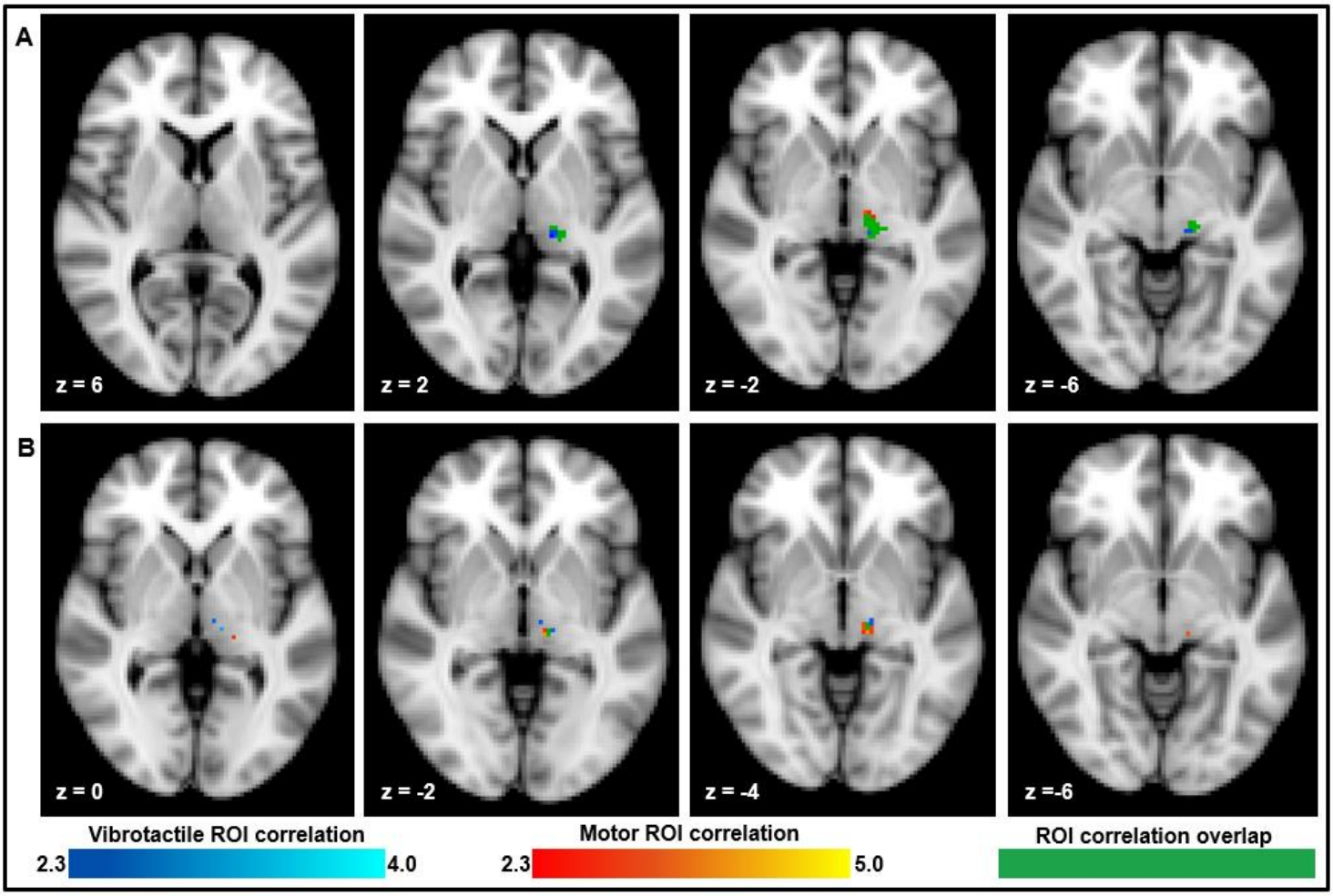

Figure 6-4: All figures are thresholded with FDR at p = 0.05. A) Controls are shown over 8 horizontal slices B) PD subjects over 4 horizontal slices

RS-fMRI for both Controls and PD groups was able to identify the motor thalamus location closer to literature-referenced Vim coordinates compared to TB-fMRI. The location comparisons are summarized in Table 6-3 and visualized in a single horizontal slice in Figure 6-5. These coordinates were farther from the lesion compared to TB-fMRI results. Both the Control and PD

groups show peak RS-fMRI coordinates to be located inferior compared to the lesion location. On average, the RS-fMRI Control and PD motor thalamus localizations were also posterior and lateral compared to both the lesion location and the literature-defined Vim coordinates.

Subject Group		Coordinates (MNI)			Distance to Lesion	Distance to Literature Peak[1]	Distance to Literature Peak[2]
		x	y	z			
Controls	**motor**	-10	-22	-4	14.1mm	5.6mm	5.1mm
	sensory	-14	-28	-4	---	---	---
Parkinson's Disease	**motor**	-12	-22	0	14.7mm	5.4mm	6.1mm
	sensory	-12	-24	-4	---	---	---

[1] Anderson et al., 2011
[2] Papavassiliou et al., 2004

Table 6-3: Summary of coordinates and distances from the Control and PD groups to each of the landmark points for this study following RS-fMRI localization results.

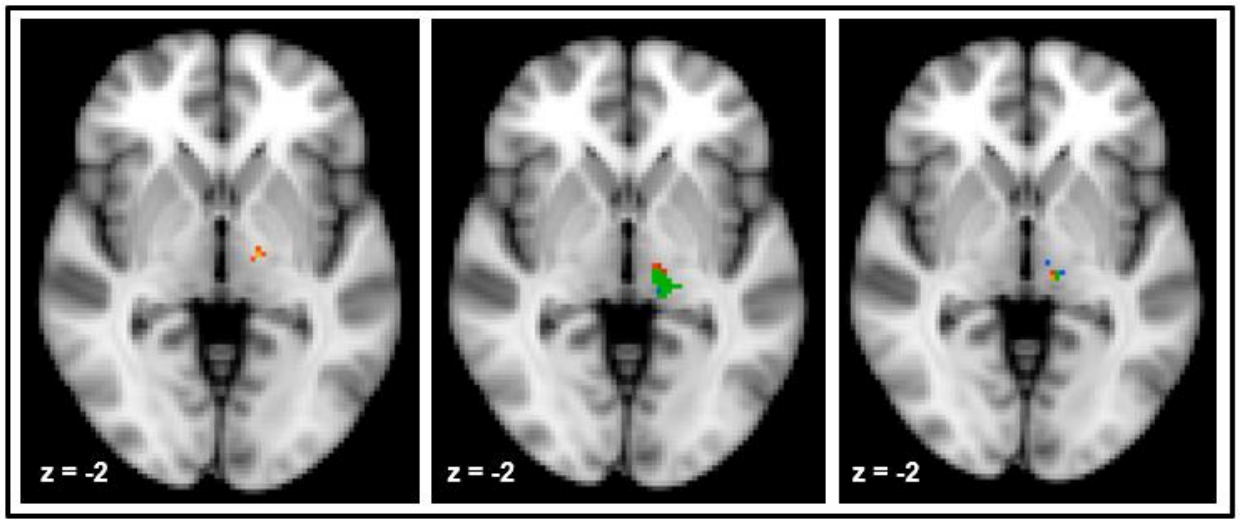

Figure 6-5: 3-panel figure shows the lesion heat map (left), and RS-fMRI correlation results from the Controls (center) and from PD subjects (right), at the same horizontal slice.

6.4 Inter-Subject Variability

Inter-subject variability within each group was analyzed by comparing the distance from each individual subject to the group mean, the lesion location and the two literature defined Vim locations. When compared to the group mean, individual RS-fMRI localization results showed significant differences between groups. Kruskal-Wallis tests (Table 6-4 – top) showed both motor and sensory thalamus location to have significant within-group variability ($\chi^2 = 6.461$, $p = 0.04$ for VPL and $\chi^2 = 7.002$, $p = 0.03$ for Vim). Comparisons from pre- and postsurgical PD groups to the Control group for sensory thalamus location (Table 6-4 – second table) showed that the Control group ($Mean_{VibroContr.} = 15.5 \pm 8.4$mm) had significantly greater distances with a much higher standard deviation and higher 95%-CI between individual subject and group mean locations compared to both the presurgical PD group ($Mean_{VibroPrePD} = 8.7 \pm 4.4$mm; $t = 3.233$, $p = 0.003$) and the postsurgical PD group ($Mean_{VibroPostPD} = 9.2 \pm 3.9$mm; $t = 2.592$, $p = 0.021$). Comparisons to the Control group for motor thalamus localization (Table 6-4 – bottom) showed that the Control group ($Mean_{MotCont.} = 14.0 \pm 7.5$mm) again had a higher mean, standard deviations, and 95%-CI range in distances compared to the postsurgical PD group ($Mean_{MotPostPD} = 6.2 \pm 1.8$mm; $t = 4.461$, $p < 0.0001$), but not compared to the presurgical PD group ($Mean_{MotPrePD} = 10.2 \pm 6.4$mm; $t = 1.643$, $p = 0.111$). TB-fMRI localization results did not find significant differences between groups in the distance between individual and group peaks.

	Kruskal-Wallis	
	X^2	p-value
Task – vibrotactile	1.355	0.852
Task – motor	3.694	0.449
Rest – vibrotactile	6.461	**0.04***
Rest – motor	7.002	**0.03**†

***Follow up Mann-Whitney U test below
†Follow up Mann-Whitney U test two tables below

Subject Group		Mann-Whitney U test†					
		n	Mean	Standard Deviation	95% Confidence Interval	t-statistic	p-value
Controls		29	15.5	8.4	11.9 | 19.2	---	---
Parkinson's Disease	presurgical *	19	8.7	4.4	6.0 | 11.3	3.233	**0.003**
	postsurgical *	7	9.2	3.9	4.3 | 14.0	2.592	**0.021**
	presurg. vs postsurg.	---	---	---	---	-0.239	0.817

*Compared to the control group
†Follow up from Kruskal-Wallis test comparing groups with Rest-vibrotactile runs

Subject Group		Mann-Whitney U test†					
		n	Mean	Standard Deviation	95% Confidence Interval	t-statistic	p-value
Controls		29	14.0	7.5	10.8 | 17.3	---	---
Parkinson's Disease	presurgical *	19	10.1	6.4	6.3 | 14.0	1.643	0.111
	postsurgical *	7	6.2	1.9	3.9 | 8.5	4.461	<**0.0001**
	presurg. vs postsurg.	---	---	---	---	-1.254	0.246

*compared to the control group
†Follow up from Kruskal-Wallis test comparing groups with Rest – motor runs

Table 6-4: *Top)* Kruskal-Wallis test looking for differences in the distance from individual subjects to group average between groups in different task and rest runs. *Second table)* Mann-Whitney U test follow up to part A to look at significant differences between groups in the Rest – vibrotactile seed run. *Bottom)* As panel B, for the Rest – motor seed run.

There was no statistically significant difference in distance between any of the groups when comparing the individual subject motor thalamus localization to the lesion location or either of the literature defined Vim locations (Table 6-5). However, the mean and standard deviation from each

group, shown in Table 6-6, indicate a large amount of variability within each group, which may undermine the feasibility of fMRI use for presurgical scanning.

	Compared to lesion		Compare to literature[1]		Compared to literature[2]	
	X^2	p-value	X^2	p-value	X^2	p-value
Task	3.093	0.542	0.417	0.981	0.585	0.965
Rest	1.241	0.538	4.591	0.101	5.508	0.064

[1] Anderson et al., 2011
[2] Papavassiliou et al., 2004

Table 6-5: Table showing results from Kruskal-Wallis tests showing nonsignificant differences in the distances from the individual subject to each landmark location (the lesion and both literature defined Vim locations), between groups.

Compared to Lesion

Subject Group		n	Mean	Standard Deviation	95% Confidence Interval
Controls	Task	26	11.0	4.9	9.0 | 13.0
	Rest	23	14.1	3.0	12.8 | 15.3
Parkinson's Disease	Task	15	12.4	3.6	10.4 | 14.4
	Rest	13	12.2	5.0	9.1 | 15.2
Essential Tremor	Task	5	14.1	4.3	8.8 | 19.3

Compared to Literature[1]

Subject Group		n	Mean	Standard Deviation	95% Confidence Interval
Controls	Task	26	11.5	5.2	9.4 | 13.6
	Rest	23	11.3	6.3	8.5 | 14.0
Parkinson's Disease	Task	15	11.4	6.0	8.1 | 14.8
	Rest	13	9.1	4.4	6.4 | 11.7
Essential Tremor	Task	5	10.4	8.1	-9.6 | 30.4

[1] Anderson et al., 2011

Compared to Literature[2]

Subject Group		n	Mean	Standard Deviation	95% Confidence Interval
Controls	Task	26	12.1	5.7	9.8 | 14.4
	Rest	23	12.8	6.1	10.1 | 15.4
Parkinson's Disease	Task	15	13.0	5.6	9.9 | 16.1
	Rest	13	9.6	4.4	6.9 | 12.3
Essential Tremor	Task	5	12.4	5.7	5.3 | 19.6

[2] Papavassiliou et al., 2004

Table 6-6: Above three tables show the mean, standard deviation, and 95% confidence interval summaries for the distance between the individual motor thalamus peak to each landmark reference point used in this thesis, separated by group.

This subject variability in motor and sensory location between groups was also further calculated using a one-way ANOVA to examine differences in each of the x-, y-, and z-directions between the Control, and the presurgical patient groups. There were no significant differences, shown in Table 6-7, in localized motor or sensory thalamus locations between groups.

		One-way ANOVA	
Axis		***F*-statistic**	***p*-value**
Task – vibrotactile	X	1.542	.216
	Y	1.204	.319
	Z	.980	.410
Task – motor	X	.246	.783
	Y	1.086	.348
	Z	.606	.551
Rest – vibrotactile	X	.481	.493
	Y	.259	.614
	Z	1.455	.236
Rest – motor	X	2.468	.125
	Y	1.051	.313
	Z	4.080	.051

Table 6-7: One-way ANOVA showing differences between Controls, ET and PD group motor and sensory thalamus parcellations, in each direction, from each TB- or RS-fMRI result.

Variability within each group was also shown using scatterplots of individual subject motor and sensory thalamus locations with references to their group peaks, the lesion location and literature Vim coordinates. While subject localization points were originally obtained from a 2 mm anatomical brain, the values used for the scatterplot include additional noise, created by adding a random value from 0 to 1 mm exclusive (less than half a voxel) to each x-, y-, and z-coordinate, to create a unique motor or sensory thalamus localization point for each subject in the scatterplot. This was only done for illustration purposes within the following scatterplots. The addition of noise better illustrates the spread of all subjects and avoids potential overlap of data from identical localization coordinates.

Figure 6-6 shows the spread of peak motor thalamus (red) and sensory thalamus (blue) locations in the Control group following task activation. In all planes, the sensory thalamus locations cluster closer together compared to the motor thalamus locations, which are generally more spread out over the whole plot. In each plot, it is possible to separate the area for motor thalamus clusters from the sensory thalamus clusters. This is only slightly evident along the Y-axis where it would be more expected, and clearly evident along the Z-axis. Both motor and sensory thalamus clusters are closer together on the x-axis and are more disperse along the z-axis.

In Figure 6-7, the motor and sensory thalamus locations are plotted for both PD and ET presurgical patients. Sensory thalamus locations are again clustered together and are localized similar to the Control group scatterplot. The motor thalamus locations in the patient population are more diffuse than in the Control group and are spread evenly compared to Figure 6-6. This may indicate changes in the thalamic motor network response in the patient population compared to in the Control group. Similar to the Control group, all results are once again clustered closer together on the x-axis and are spread farther apart on the z-axis.

Plotted thalamic peaks from RS-fMRI for the Controls and PD group can be seen in Figures 6-8 and 6-9 respectfully. Based on visual inspection of trends in the scatterplots for both groups, the motor and sensory localizations are difficult to distinguish from each other using seed-based RS-fMRI. The scatterplots show a similar range in data spread on each axis, compared to the results from TB-fMRI.

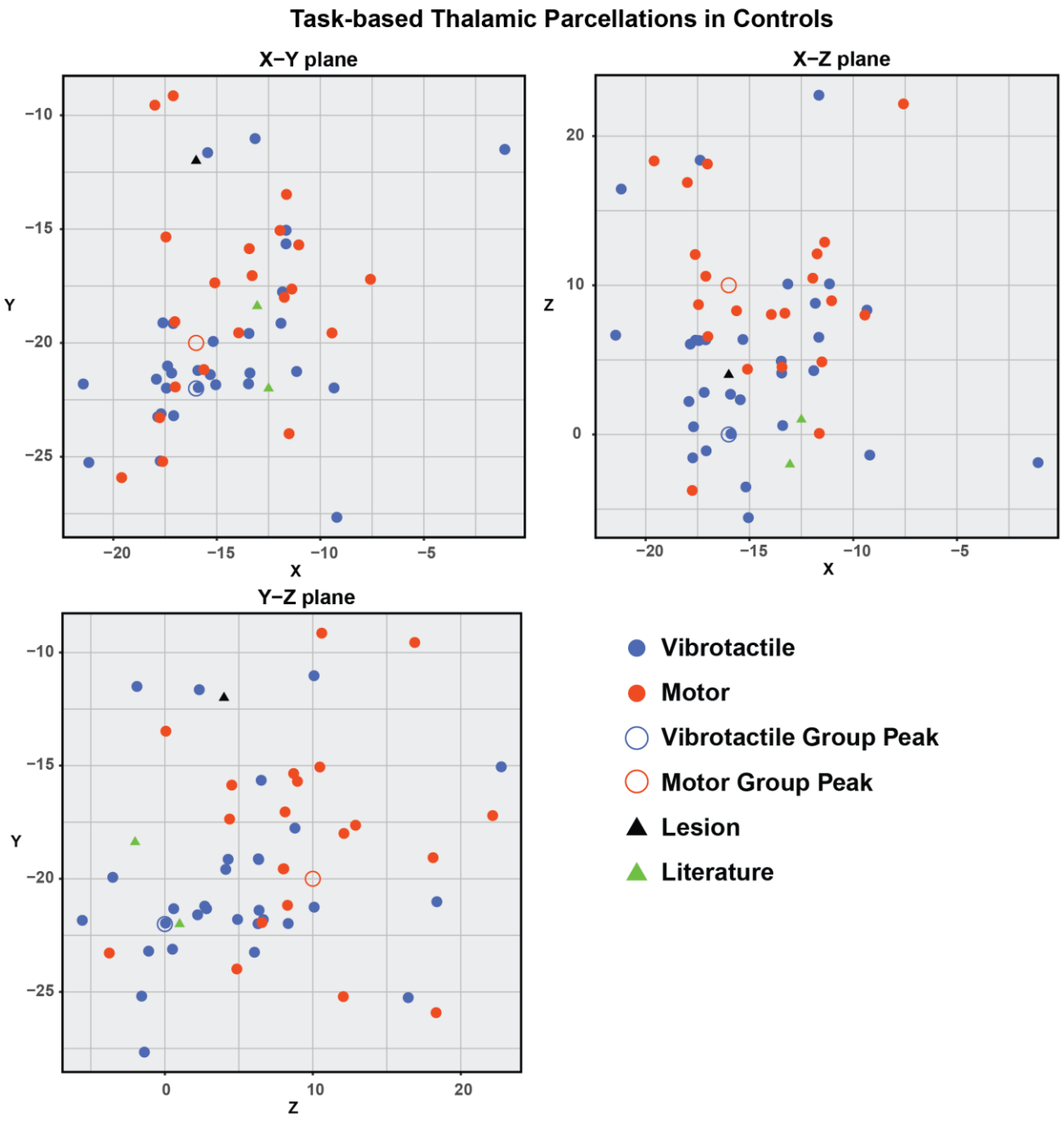

Figure 6-6: Scatterplot showing individual subject thalamic localizations using TB-fMRI in Controls, compared to group localization, lesion, and literature coordinates. Motor (red) and sensory thalamus (blue) locations following task-based fMRI can be seen clustered somewhat separately along the Y-axis, and more evidently separated along the Z-axis.

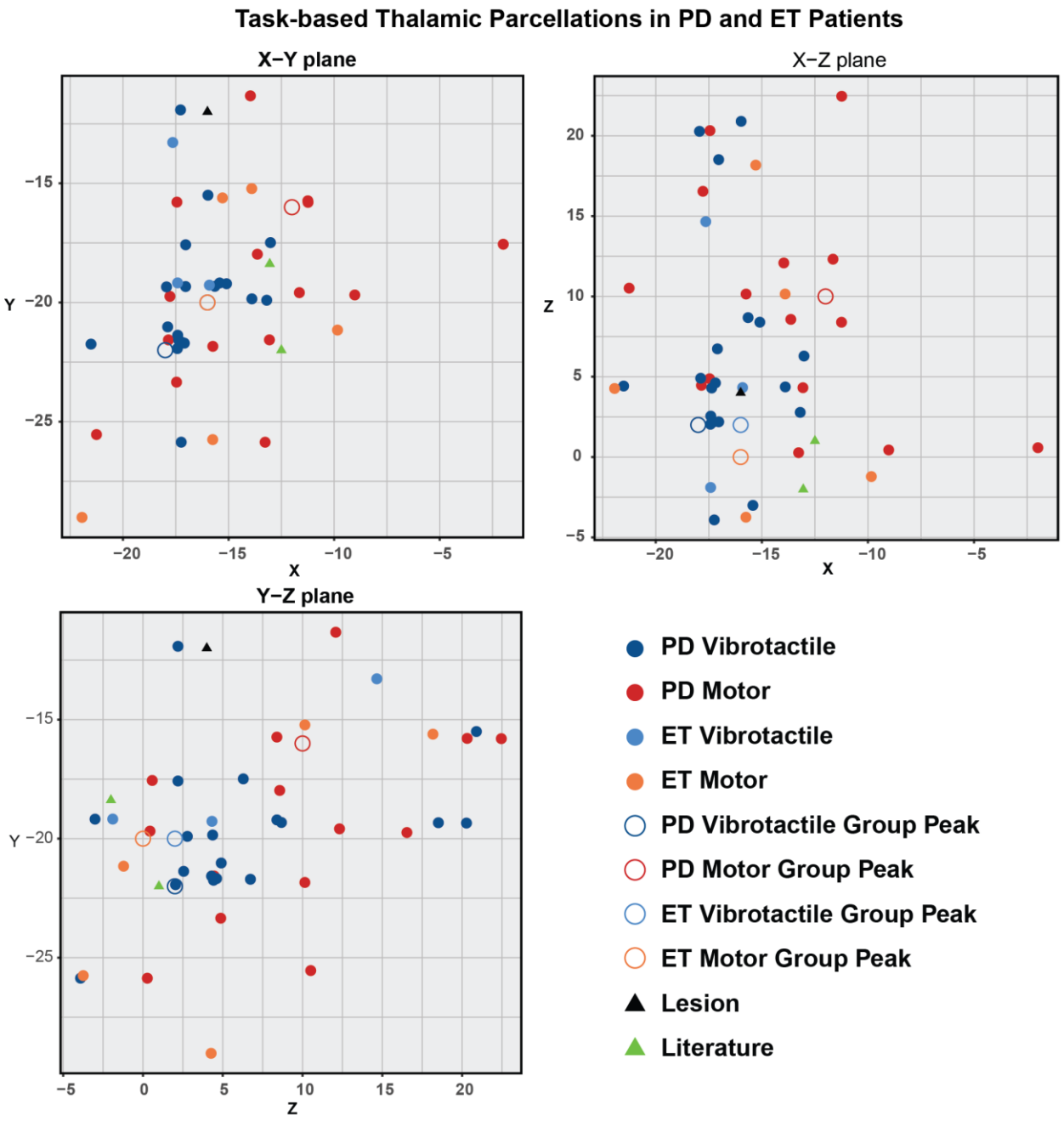

Figure 6-7: Scatterplot showing individual subject thalamic localizations using TB-fMRI in PD and ET patients, compared to group localization, lesion, and literature coordinates. PD vibrotactile responses are clustered close to one another. This is not seen in the motor thalamic response, unlike the results from the Control group. It is difficult to discern cluster patterns in the ET group as there are fewer results.

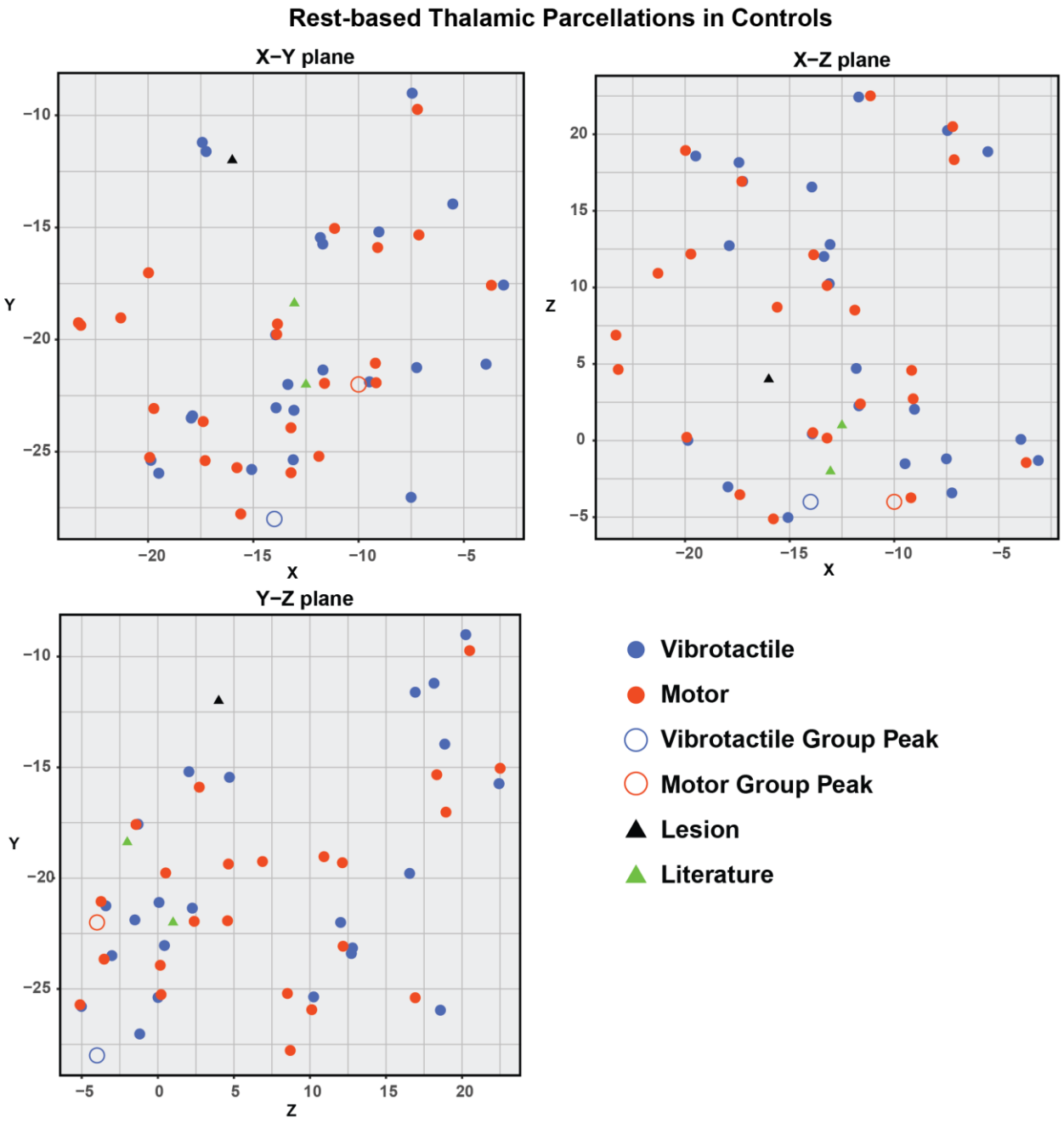

Figure 6-8: Scatterplot showing individual subject thalamic localizations using RS-fMRI in Controls, compared to group localization, lesion, and literature coordinates. Motor and sensory thalamus RS-fMRI seed correlations are more difficult to discern from one another compared to the results from TB-fMRI in the Controls (Figure 6-6).

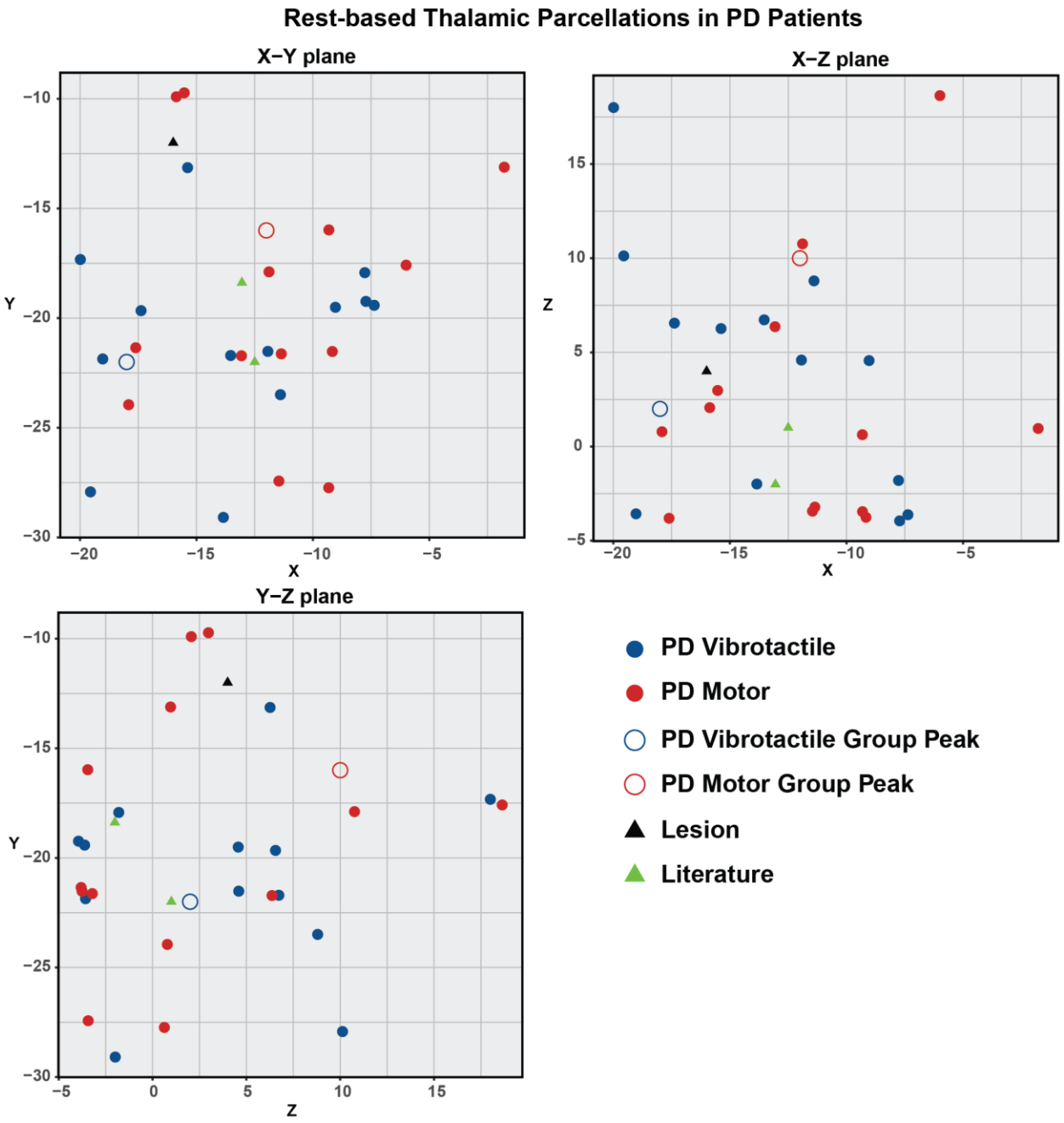

Figure 6-9: Scatterplot showing individual subject thalamic localizations using RS-fMRI in PD patients, compared to group localization, lesion, and literature coordinates. Similar to the previous figure, motor and sensory thalamus localizations in the PD patients are also more difficult to discern from one another compared to the results from TB-fMRI (Figure 6-7).

Compared to the TB-fMRI counterparts, RS-fMRI was able to localize the motor thalamus in a higher percentage of total subjects. After FDR, the RS-fMRI defined motor thalamus could be localized in 82.6% of Control subjects and 69.2% of presurgical PD subjects. In comparison, TB-fMRI produced successful motor thalamus localization results in 72% of Controls, 60% of presurgical ET patients, and only 41.2% of presurgical PD patients, following the motor task. When the FDR correction was removed, and all fMRI z-statistic maps were thresholded to $p = 0.05$ (uncorrected), this resulted in successful TB-fMRI motor thalamus localization in 88% of Controls, 100% of pre-surgical ET patients, and 88.2% of pre-surgical PD patients and RS-fMRI motor thalamus localization in 100% of subjects across all groups (Table 6-8).

The sensory thalamus was also localized in a larger percentage of total subjects using RS-fMRI compared to TB-fMRI. RS-fMRI was able to identify the sensory thalamus component in 91% of Controls, and 84.6% of PD patients after FDR correction, and 100% of patients without FDR correction. Similar to the motor thalamus counterpart, TB-fMRI had less success localizing the sensory thalamus, only succeeding in identifying the sensory thalamus in 51.7% of Controls, 15.8% of PD patients and 14.3% of ET patients after FDR corrections. These percentages, particularly in the patient population, are much lower than the motor component.

Subject Group		Task-based fMRI		Resting-state fMRI	
		% subject correlation (FDR)	% subject correlation (p = 0.05)	% subject correlation (FDR)	% subject correlation (p = 0.05)
Motor Thalamus	Controls	18/25 – 72%	22/25 – 88%	19/23 – 82.6%	23/23 – 100%
	Parkinson's Disease	7/17 – 41.2%	15/17 – 88.2%	9/13 – 69.2%	13/13 – 100%
	Essential tremor	3/5 – 60%	5/5 – 100%	---	---
Sensory Thalamus	Controls	15/29 – 51.7%	29/29 – 100%	21/23 – 91.3%	23/23 – 100%
	Parkinson's Disease	3/19 – 15.8%	19/19 – 100%	11/13 – 84.6%	13/13 – 100%
	Essential tremor	1/7 – 14.3%	3/7 – 42.9 %	---	---

Table 6-8: Frequency of Vim localization success between TB-fMRI and RS-fMRI in all groups

6.5 Thalamic Activation and Connectivity

The strength of TB-fMRI activation and RS-fMRI connectivity in the patient population was measured by extracting the z-statistic in the peak voxel within the thalamus and comparing it to the Control group. There were significant group differences in thalamic activation (Table 6-9 – top) associated with the motor (χ^2 = 11.664, p = 0.02) and vibrotactile tasks (χ^2 = 12.332, p = 0.015). The vibrotactile task produced decreased thalamic activation in both the presurgical PD group (t = 2.377, p = 0.022) and the presurgical ET group (t = 3.502, p = 0.009) (Table 6-9 – second table). The motor task also produced a decrease in thalamic activation, however only in the presurgical PD group (t = 2.065, p = 0.046) (Table 6-9 – third table). There was also a difference in activation between the presurgical and postsurgical ET groups, where postsurgical thalamic activation increased significantly (t = 2.839, p = 0.017). There were no other differences in thalamic task activation between pre- and postsurgical patient groups.

RS-fMRI also showed a decrease in thalamocortical correlation in the presurgical PD patients (t = 3.443, p = 0.002) compared to the Control group, however there was no significant differences in this correlation between the Control group and the postsurgical group, or between the pre- and post-surgical PD patient groups (Table 6-9 – bottom).

	Kruskal-Wallis	
	X^2	**p-value**
Task – vibrotactile	12.332	**0.015***
Task – motor	11.664	**0.020**†
Rest – vibrotactile	1.028	0.598
Rest – motor	8.675	**0.013**‡

*****Follow up Mann-Whitney U test below
† Follow up Mann-Whitney U test two tables below
ǂ Follow up Mann-Whitney U test three tables below

Subject Group		Mann-Whitney U test†					
		n	**Mean**	**Standard Deviation**	**95% Confidence Interval**	**t-statistic**	**p-value**
Controls		29	3.8	1.3	3.3 | 4.3	---	---
Parkinson's Disease	presurgical *	19	3.0	0.9	2.6 | 3.5	2.377	**0.022**
	postsurgical	7	3.2	1.0	2.2 | 4.1	---	---
	presurg. vs postsurg.	---	---	---	---	-0.341	0.740
Essential Tremor	presurgical *	7	1.3	1.8	-0.4 | 2.9	3.502	**0.009**
	postsurgical	5	3.6	1.1	2.4 | 4.7	---	---
	presurg. vs postsurg.	---	---	---	---	-2.829	**0.017**

*Compared to the Control group
†Follow up from Kruskal-Wallis test comparing groups with Task-vibrotactile runs

Subject Group		Mann-Whitney U test†					
		n	**Mean**	**Standard Deviation**	**95% Confidence Interval**	**t-statistic**	**p-value**
Controls		25	4.0	2.0	3.2 | 4.9	---	---
Parkinson's Disease	presurgical *	17	2.9	1.6	2.1 | 3.7	2.065	**0.046**
	postsurgical	7	2.9	0.7	2.3 | 3.6	---	---
	presurg. vs postsurg.	---	---	---	---	-0.084	0.934
Essential Tremor	presurgical *	5	3.8	1.8	1.5 | 6.1	0.253	0.808
	postsurgical	5	1.5	1.3	-0.2 | 3.1	---	---
	presurg. vs postsurg.	---	---	---	---	2.324	0.051

*compared to the Control group
†Follow up from Kruskal-Wallis test comparing groups with Task – motor runs

Subject Group		Mann-Whitney U test†					
		n	**Mean**	**Standard Deviation**	**95% Confidence Interval**	**t-statistic**	**p-value**
Controls		29	4.5	0.9	4.1 | 4.9		
Parkinson's Disease	presurgical *	19	3.6	0.7	3.2 | 4.0	3.443	**0.002**
	postsurgical	7	4.0	0.7	3.2 | 4.9	---	---
	presurg. vs postsurg.	---	---	---	---	-1.254	0.246

*compared to the Control group
†Follow up from Kruskal-Wallis test comparing groups with Rest – motor runs

Table 6-9: A) Kruskal-Wallis test examining the peak z-stat value in the thalamus between groups in different task and rest runs. B) Mann-Whitney U test follow up to part A to look

at significant differences between groups after the motor task C) As panel B, for differences between groups after the vibrotactile task D) As previous, for differences in correlation between group from the motor seed in RS-fMRI

6.6 Third Ventricle Size

There was a significant difference in third ventricle size in the y-direction in pre-surgical PD patients compared to the Control group ($Mean_{Controls}$ = 35.0 ± 2.6mm vs $Mean_{PD}$ = 36.8 ± 2.4mm, t = -2.529, p = 0.015). There were no significant differences in total third ventricle volume, x-direction or z-direction, or between Controls and ET patients, or between pre- and post-surgical patient groups (Table 6-10).

Subject Group		Mean (mm)	Standard Deviation (mm)	t-statistic	p-value
Controls	Volume	1403.8	432.5	---	---
	X	7.0	1.3	---	---
	Y	35.0	2.6	---	---
	Z	22.1	2.9	---	---
Presurgical Parkinson's Disease *	Volume	1519.5	409.6	-0.984	0.331
	X	7.1	1.2	-0.413	0.691
	Y	36.8	2.4	-2.529	**0.015**
	Z	22.1	2.8	-0.101	0.920
Postsurgical Parkinson's Disease †	Volume	1420.5	179.7	0.856	0.402
	X	7.2	0.8	-0.060	0.953
	Y	38.0	3.3	-0.825	0.438
	Z	23.0	2.6	-0.698	0.503
Presurgical Essential Tremor *	Volume	1619.6	373.2	-1.415	0.182
	X	7.3	0.7	-0.725	0.476
	Y	36.3	3.0	-1.051	0.319
	Z	23.1	3.4	-0.824	0.430
Postsurgical Essential Tremor †	Volume	1837.7	564.0	-0.822	0.435
	X	7.6	1.6	-0.585	0.578
	Y	36.3	3.4	-0.047	0.963
	Z	25.5	6.5	-0.813	0.443

* Compared to Controls
† Compared to presurgical equivalents

Table 6-10: Separate comparisons between groups for each category: Volume, x, y, and z directions

However, significant changes in the y-direction may not affect Vim localization as the thalamus is located superiorly and laterally adjacent to the third ventricle. The x-, y-, and z-direction third ventricle dimensions were used as a covariate with the one-way ANOVA results from Table 6-5. ANCOVA results, shown in Table 6-11, showed no significant differences in localized motor or sensory thalamus locations between the Controls, and presurgical patient groups.

		One-way ANCOVA	
		F-statistics	**p-value**
Task – vibrotactile	X	1.517	.223
	Y	1.157	.336
	Z	1.400	.255
Task – motor	X	.227	.798
	Y	.842	.439
	Z	.605	.551
Rest – vibrotactile	X	.444	.510
	Y	.496	.486
	Z	1.445	.286
Rest – motor	X	2.235	.144
	Y	.508	.481
	Z	4.108	.051

Table 6-11: One-way ANCOVA results using third ventricle dimensions as a covariate in each of the x-, y-, and z-directions

CHAPTER 7: **DISCUSSION**

Accurate pre-surgical localization of thalamic nuclei may decrease operating times by reducing time dedicated to electrode exploration, reduce post-surgical complications and improve clinical outcome. As shown in this thesis, fMRI can localize the Vim in the Control group as well as in PD and ET patients.

7.1 Group Localization Results

In the Control and PD groups, TB-fMRI results localized the motor thalamus location closer to the peak of the thalamotomy lesion heat map, compared to the location of the Vim identified by literature sources. In both groups, the identified motor thalamus was slightly lateral (<4mm) compared to the literature defined Vim location, but on the same x-axis as the lesion. Both groups' motor thalamus located 8mm posterior to the lesion, yet between the two literature defined Vim locations on the y-axis. The only direction where the Control and PD group differ significantly in group motor thalamus locations is in the z-direction, where the Control localization is far superior from both the literature locations (>9mm), and the lesion location (6mm). Contrasted to this, the PD group z-direction motor thalamus lay between the literature defined Vim locations and was only 4mm from the lesion.

The motor thalamus location identified in the ET group was much closer to the two literature Vim locations (3.9mm and 4.2mm) compared to the lesion location (8.9mm), but nonsignificant activation post-thresholding prevents definitive conclusions. This may be due to changes in thalamic sensorimotor activation in ET patients (discussed in a later section), however, a larger sample size would be necessary to robustly confirm such a hypothesis. Sensory thalamus locations were only compared to the respective motor thalamus localization results based on

histological atlases, as there are few literature sources that target the VPL using functional or structural neuroimaging. In the Control and PD groups, the targeted sensory thalamus lay posterior and inferior to the localized motor thalamus, which was the expected VPL location, relative to the Vim.

RS-fMRI results yielded different localization results compared to TB-fMRI. RS-fMRI motor thalamus in both the Controls and the PD groups were medially located compared to both the lesion (6mm and 4mm respectively) and the literature Vim locations (3mm and 1mm respectively). In the y-direction, both groups were 10mm from the lesion, however, they were only 5mm from one literature Vim location, and at the same y-coordinate as the other literature Vim location. Opposite to the results in TB-fMRI, the Controls were far inferior rather than superior from the lesion location (8mm away) and the literature locations (5mm from the farthest literature location). The RS-fMRI results in the PD group also showed this pattern – PD motor thalamus localizations using RS-fMRI were 5mm inferior to the lesion, but once again, between the literature defined Vim locations. The sensory thalamus localization in the Control group showed the expected superior-posterior location compared to the motor thalamus localization in the same group, however, this was not the case in the PD group.

It is difficult to discern whether TB-fMRI or RS-fMRI based localization is a better representation of the actual Vim or VPL location. Control and PD subjects' TB-fMRI results were about equally far from the lesion location in the heat map and the literature locations, while ET subjects, were much closer to the literature defined Vim locations than the heat map lesion locations. RS-fMRI results were closer to the literature Vim locations and farther from the lesion location in the heat map but were unable to identify the sensory thalamus relative to the motor thalamus in the PD group. One problem with these comparisons is the range of potential Vim

locations provided within different literature sources. The two literature defined Vim locations are 4.7mm apart themselves, while each of these is located approximately 10mm from the lesion heat map defined from our own postsurgical patient group.

One potential explanation for these differences is the varying anatomical Vim location between different populations. Human brains are variable between individuals even within the same group, and these differences depend on may factors, including age, gender, and ethnicity. While this study centered around the use of the MNI-152 2mm template to standardize all brain transformations, the use of different templates representative of different populations should be considered (Tang et al., 2010). Examples may include comparisons to the Chakravarty atlas or the Morel atlas, which define thalamic subnuclei. However, as previously noted, these atlases also include their own variability in nuclei location and definition (Horn et al., 2017).

Despite these differences in brain variability, the lesion heat map localization and two literature-defined Vim locations are both likely to be clinically effective locations for tremor alleviation. The key caveat to maintain this effectiveness remains the avoidance of the VPL and surrounding sensory area (Papavassiliou et al., 2004). With the TB-fMRI results of each group more consistently separating motor thalamus from sensory thalamus locations, TB-fMRI may be a preferred choice for presurgical targeting based on the group-fMRI localization results.

7.2 Individual Subject Localization

With respect to presurgical planning, individual subject localization may be more relevant than group-fMRI results. Comparing x-, y-, and z-coordinates of each TB-fMRI and RS-fMRI motor and sensory thalamus coordinate between groups showed that there was no statistical difference in the localized motor or sensory thalamus position in the patient population compared

to Controls. Thus, motor disorders may change aspects such as network activation or the strength of thalamocortical connectivity, but not the position of the localized motor or sensory thalamus area. This was also reflected in the comparisons of the averaged individual subject motor thalamus localization to each of the landmark comparison locations. The mean distances presented in Table 6-6 are comparable to the peak motor thalamus to literature Vim or lesion distance found using group analysis; in the TB-fMRI results, these are within 2mm. The exception is the ET group where averaged individual subject motor thalamus localizations are much farther than the peak from the group analysis. The large variance may be due to the small sample size of this subject group.

It is evident from the scatterplots that TB-fMRI succeeded in differentiating the motor thalamus from the sensory thalamus, where RS-fMRI did not. As already noted in the group results, the TB-fMRI sensory thalamus locations were posterior and inferior to the motor thalamus locations in each group, as would be expected based on histological findings. One reason RS-fMRI may have failed here is due to seed choice. While the motor and somatosensory systems mostly differ in function, they are anatomically very close. The two seeds to distinguish the motor and somatosensory systems (within BA4 and BA3) may not have the specificity to separate these networks. This problem is accentuated by the fact that these seeds were chosen within the MNI 152 template, made by averaging brains from healthy young adults. While the seeds were linearly and nonlinearly transformed to the individual subject brain, any inaccurate registration not caught by quality assurance checks may result in a bias from the motor to somatosensory network, or vice versa. This issue echoes the previous section regarding the problems with variable neuroanatomy. Higher resolution structural and functional imaging, and subject specific cortical segmentations

may be able to mitigate this problem in the future. Meanwhile, these findings support the use of TB-fMRI to separate the Vim from the VPL.

One surprising discovery is the significantly larger mean distance and standard deviation between the individual subject peaks and the group mean in the Control group, compared to the other groups, in RS-fMRI results. Upon close examination of the scatterplot, the group motor and sensory thalamus localizations are inferior and posterior compared to the mean of the individual motor and sensory peaks. This misrepresentation is also reflected in Table 6-6. Distances from the averaged individual subject RS-fMRI motor thalamus localization to the two literature Vim locations (Controls: 11.3 ± 5.2mm and 12.8 ± 6.1mm; PD: 9.1 ± 4.4mm and 9.6 ± 4.4mm respective to the two literature locations) were much higher compared to the group analysis RS-fMRI motor thalamus localizations to the same two literature Vim locations (Controls: 5.6mm and 5.1mm; PD: 5.4mm and 6.1mm). There was also a large difference between averaged individual subject RS-fMRI motor thalamus localizations compared to the lesion (Controls: 14.1 ± 3.0mm; PD: 12.2 ± 5.0mm) and the group analysis RS-fMRI motor thalamus localization compared to the lesion (Controls: 14.1mm; PD: 14.7mm).

The skewed group motor and sensory thalamus localizations could be the result of cortical connectivity with regions proximal to the thalamus, which also participate in motor functions. The group RS-fMRI motor thalamus localization in the Control group is close to the adjacent zona incerta (ZI), illustrated in Figure 7-1. The ZI is a horizontally elongated area located inferior to the thalamus, adjacent to the thalamic reticular nucleus which itself wraps around much of the thalamus. The ZI also extends over the subthalamic nucleus (STN). The ZI receives afferents from the GPi, parts of the substantia nigra, the cerebellum, and the cortical motor, associative and limbic areas. The ZI sends out efferents to the thalamic ventral anterior nucleus, thalamic VL, and to

many other predominately subcortical structures (Mitrofanis, 2005; Plaha, Khan, & Gill, 2008). The ZI is primarily composed of GABAergic neurons, and so it predominately modulates the basal ganglia output nuclei, neurons within the cerebellothalamocortical loop, and the brainstem. With respect to the sensorimotor networks, the ZI is involved in maintaining posture and locomotion via its connections within the cerebellum, red nucleus, and cervical and lumbosacral regions of the spinal cord, and the pontine nuclei, the majority of these within the caudal ZI (cZI) (Mitrofanis, 2005). More recent studies have implicated its role within the cerebellothalamocortical loop in tremor generation, and have found positive preliminary results for the use of the cZI as another target for DBS (Plaha et al., 2008).

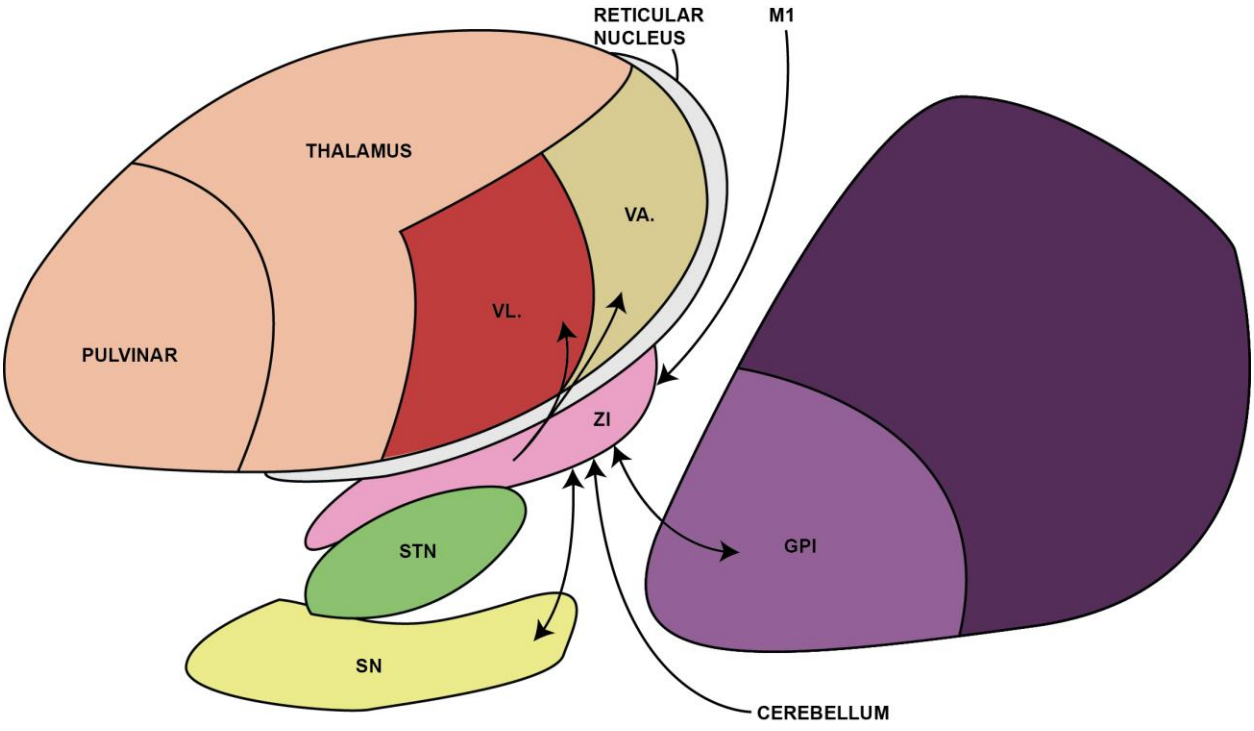

Figure 7-1: Schematically illustrates location of ZI, as well as some of its major afferents and efferents as it pertains to motor and sensory function. Adapted from Plaha et al., 2008.

The cZI's connectivity within the resting state sensorimotor network have not been studied. It would be reasonable to assume some correlated time courses between the cZI and the motor

cortical regions, given its structural connections and related motor functions. Significant functional connectivity has been found between the adjacent STN and the primary motor cortex, with increased connectivity in patients with PD (Baudrexel et al., 2011). The STN is another structure implicated in tremor circuits, more specifically in PD patients. It is a frequent target for bilateral DBS in patients with tremor and other PD features (Rodriguez-Oroz et al., 2005; Rodriguez et al., 1998).

Connectivity to structures adjacent to the ventral thalamus may have affected the localization ability in group-level modeling. FSL-FLAME was the model used to estimate the inter-subject effects within the group. While the results seen do not appear as an average or fixed effects model of our sample, the mixed effects model incorporates random effect variance to extrapolate the results representative of a population rather than a subset. These random effect variances are drawn from the variances brought up from the first-level parameter estimates. Individual subject variances in the resting-state Control group may have skewed the group estimate inferior and posteriorly compared to TB-fMRI and the patient groups, due to these other RS-fMRI correlations. In combination with the use of the thalamic mask to isolate the relevant thalamic RS-fMRI correlation, the group level analysis may have been biased towards the posterior edge of the thalamic mask, leading to the current results. These differences were not seen in the RS-fMRI PD group. This could be due to a difference in subcortical connectivity in PD, such as between the motor cortex, and the STN or cZI.

As a solution to this problem, the center of mass instead of the peak voxel could potentially be used for comparisons between individual and group, and between groups. This may be less representative of the combined subject pool and would be biased by thresholding techniques, which would change the center of mass.

7.3 Thalamic Parcellation Reproducibility

Being able to consistently reproduce fMRI analysis to localize the Vim is also important to assess the feasibility of fMRI for presurgical mapping. The results showed that both with and without FDR correction RS-fMRI more consistently produced motor and sensory thalamus locations. After FDR correction, it was easier to locate the motor and sensory thalamus in the Controls compared to the patient groups with either TB-fMRI or RS-fMRI.

This result may indicate a trend of decreased TB-fMRI thalamic activation and decreased RS-fMRI corticothalamic connectivity in the patient population. In the TB-fMRI results, we looked directly at the strength of activation in the thalamus by comparing thalamic z-statistic values and found a significant decrease in activation in presurgical PD subjects after all tasks, and presurgical ET subjects after the vibrotactile task. This was not surprising as the group TB-fMRI results from the PD group showed a consistently smaller volume of thalamic activation compared to in the Controls, and group TB-fMRI motor thalamus localization results from the ET group were equally small in activation volume, and the TB-fMRI sensory thalamus localization was statistically non-significant.

RS-fMRI results also showed a decrease in corticothalamic connectivity between the Control group and the presurgical PD group using the motor seed, but not the vibrotactile seed. This is surprising as the group PD results showed much smaller volumes of thalamic correlation after both the motor and the sensory task.

The RS-fMRI ROI analyses show that the diseased state may itself be a moderate confounder to using fMRI as a tool for thalamic localization. Using a less stringent threshold such as removing the multiple comparisons for either TB-fMRI may be an effective starting point for

further electrophysiology refinement. While RS-fMRI may also be used, it should be limited to cases where the patient is incapable of performing the tasks necessary for TB-fMRI analysis.

7.4 Study Design Limitations

The study suffers from a few drawbacks. Older subject groups such as this one may have more inconsistencies in their reaction to motor tasks and vibrotactile stimulus. Aging also has a large effect on structural brain changes such as decreasing cortical thickness (Thambisetty et al., 2010), decreases in whole brain, temporal lobe and hippocampal volume, increases in ventricle size (Scahill et al., 2003), and decreases in thalamic volume (Sullivan, Rosenbloom, Serventi, & Pfefferbaum, 2004). While changes in third ventricle size and dimensions did not affect our data, this may be a factor in larger sample sizes, particularly in older populations, and those with dementia associated with PD. Other changes in brain volume will affect the ability to isolate resting-state networks by confounding the use of an anatomical atlas-based seed, based on the MNI 152 brain template. Often, age-matched controls are provided to reduce the amount of variability in the study. However, due to limited number of patients, particularly in the ET group, there is a statistically significant difference in age between the Control group and the ET group ($Mean_{Controls}$ = 59.8 ± 9.4, $Mean_{preET}$ = 68.1 ± 7.0, t = -2.310, p = 0.026). The unbalanced number of subjects we have in each group also affects the power within the statistical comparisons between groups.

As previously mentioned, seed-based analysis also requires *a priori* selection of a seed, which introduces certain biases to analysis, such as seed size and location. While seed-based analysis was chosen to provide a direct answer to a direct question asked on the motor and somatosensory networks, in reality, these seeds are influenced by their surrounding structures, creating spatial confounds. As previously discussed, the close locations of the two seeds may bias

the other due to spatial proximity, in that these defined locations may not be so different from one another. The choice of a larger or smaller seed, or small movements of chosen BA3 or BA4 seeds used in this study, may also change the observed network, and instead lead to any number of subnetworks. As an example, Cole et al., demonstrated the difference in single subject network identification between 3 different resting-state default mode network (DMN) seeds and the ICA equivalent. The results showed varied overlap amounts of correlation within the whole DMN (Cole, Smith, & Beckmann, 2010). Seeds were also defined in an atlas and transformed into individual subject space to remove the bias of potentially shifting this seed in each subsequent subject, however, inter-subject differences in networks would also result in similar differences shown in Cole et al. As a consequence, the biases of seed-based correlation may have influenced the results of this study. The choice to use seed-based correlation to acquire a very definitive answer to the proposed question still stands as an appropriate method for this particular analysis.

The EPI sequence used for fMRI acquisition are affected by magnetic field inhomogeneities and are susceptible to image distortions. These distortions generally occur at tissues neighbouring interfaces with air in the sinuses. While these areas do not directly affect the sensorimotor cortices and the thalamus, as it pertains to this thesis, misregistration of individual subject fMRI scans may skew the location of the motor thalamus, especially due to its small size relative to other larger structures. To mitigate this, careful visual quality assurance was performed on each registration. However, registration may be further improved by field mapping or bias field corrections.

The low resolution of functional imaging protocol used here prevents localization with more precision than 4mm due to the imaging voxel size. Because of this, images may also suffer from partial volume artefacts due to the small size of the Vim. This may cause some inaccuracies

in BOLD image-based localization. The choice to not smooth the data was an attempt to minimize these errors, however, not smoothing can increase the chance of type II errors in the statistical analysis.

Lastly, some analysis was limited by the lack of clinical data available. For example, lesion size is highly variable depending on time post-surgery. Follow up, including patient outcome post-surgery was also not factored into the analysis here, but should be included in future analysis of this dataset.

7.5 Future Directions

A wide variety of future analysis could also be done with this dataset. In our collected dataset, many of the subjects are still awaiting thalamotomy, and thus, only a small portion of potential post-surgical subjects were included in this study. Many analyses with post-surgical subjects were excluded due to insufficient sample size. For example, longitudinal fMRI data could be examined to identify changes in functional connectivity as a result of the thalamotomy. The current literature regarding reorganization of functional networks post-surgical treatment is limited. A single case reported increased BOLD signals post-DBS using fMRI in different cortical regions, but only in reference to electrode placement within the STN rather than the thalamus (Perlmutter & Mink, 2006).

Combining multi-modal imaging has also become popular and many of the subjects have datasets which not only include the anatomic, TB-fMRI, and RS-fMRI datasets used in this study, but also DTI and magnetization transfer (MT) image data as well. To further investigate thalamic nuclei targeting, DTI has been commonly used as a stand-alone imaging modality. A large drawback seen in previous DTI-based thalamic parcellation shows that cortical borders become

fuzzy due to overlapping white matter tracts and indistinct borders between thalamic nuclei (Johansen-Berg et al., 2005). This is particularly true when DTI seed inputs are in the cortex, as many of the cortical tracts leading into the thalamus connect to other subcortical regions. A preliminary study using this dataset has combined the DTI data with the TB-fMRI, using fMRI activation areas as a seed for DTI (Ghaderi, Sadikot, Campbell, & Pike, 2012). Combining DTI with resting-state fMRI provides a functional component to structural brain mapping. An overview of many studies shows that resting-state functional connectivity is relatively well correlated to structural connectivity (Damoiseaux & Greicius, 2009). A study comparing DTI with an fMRI map within the cortex showed the importance in defining thalamocortical connectivity specifically, with both structural and functional imaging (D. Zhang et al., 2010). While they showed that there was overlap between the two modalities, motor and premotor cortex showed the most differences, with only 36% of the DTI map overlapping the functional map. These differences could be attributed to the differences in resolution between DTI and fMRI acquisition. Differences may also be due to seeding methods and ROI definitions.

CHAPTER 8: **CONCLUSIONS**

In this study, TB-fMRI and RS-fMRI methods were used to localize motor and sensory regions of the thalamus relevant to tremor relieving neurosurgery. The localized motor thalamus was then compared to thalamotomy lesion locations and literature-based Vim coordinates. Both group analysis using a mixed-effects model and a simple average of all individual subject motor thalamus locations were used for this comparison. While both methods have their benefits and drawbacks, the averaged individual subject thalamic nuclei may be a better representation of potential clinical applications. The TB-fMRI results were generally found to be >10mm away from the lesion locations and literature Vim locations for all groups. Similar results were found for the group analysis of the TB-fMRI data. Compared to the post-surgical lesion site, TB-fMRI was seen to localize the motor thalamus within 11.0 ± 4.9mm in Controls, 12.4 ± 3.6mm in PD patients and 14.1 ± 4.3mm ET patients. Compared to two literature-defined Vim coordinates, the Control group measured 11.5 ± 5.2mm and 12.1 ± 5.7mm respective to each literature location, the PD group measured 11.4 ± 6.0mm and 13.0 ± 5.6mm, and the ET group measured 10.4 ± 8.1mm and 12.4 ± 5.745mm. RS-fMRI results showed the greatest difference between averaged individual subject and group analysis thalamic localizations. The motor thalamus was localized 14.1 ± 3.0mm from the surgical lesion site in the Controls, and 12.2 ± 5.0mm in the PD patients. Compared to the two literature defined Vim coordinates, the Control motor thalamus measured11.3 ± 6.3mm and 12.8 ± 6.1mm away from each of the literature Vim locations respectively, while the PD motor thalamus was at 9.1 ± 4.4mm and 9.6 ± 4.4mm away. Despite these generally large distances, TB-fMRI was still able to better differentiate the motor and sensory thalamus (nominally Vim and VPL), which is important to minimize side effects associated with the surgery. Parcellating the Vim and VPL in the patient population compared to the Control group was less successful overall using either

TB-fMRI or RS-fMRI, however, in the patients who did exhibit a successful localization, the actual location was not affected by the presence of disease.

Accounting for variability in the size and shape of the thalamus between individuals, and the inconsistency between common atlases, fMRI may allow presurgical localization of thalamic targets to be more uniquely tailored to each patient. Given the results from this study, TB-fMRI may be the more reliable method for Vim targeting due to its better precision. RS-fMRI may be an option if the patient is not capable of performing the associated tasks for TB-fMRI. In both cases, higher resolution functional imaging would be beneficial if available for use. In either case, further electrode refinement is still necessary to identify the correct structure before a thalamic lesion or DBS electrode placement. Future work is needed to better refine this technology before clinical usage.

REFERENCES

Akram, H., Dayal, V., Mahlknecht, P., Georgiev, D., Hyam, J., Foltynie, T., … Zrinzo, L. (2018). Connectivity derived thalamic segmentation in deep brain stimulation for tremor. *NeuroImage: Clinical*, *18*(January), 130–142. https://doi.org/10.1016/j.nicl.2018.01.008

Anderson, J. S., Dhatt, H. S., Ferguson, M. a, Lopez-Larson, M., Schrock, L. E., House, P. a, & Yurgelun-Todd, D. (2011). Functional Connectivity Targeting for Deep Brain Stimulation in Essential Tremor. *American Journal of Neuroradiology*, *32*(10), 1963–1968. https://doi.org/10.3174/ajnr.A2638

Bach, J.-P., Ziegler, U., Deuschl, G., Dodel, R., & Doblhammer-Reiter, G. (2011). Projected Numbers of People with Movement Disorders in the Years 2030 and 2050. *Movement Disorders*, *26*(12), 2286–2290. https://doi.org/10.1002/mds.23860

Barrett, K., Brooks, H., Boitano, S., & Barman, S. (2010). *Ganong's Review of Medical Physiology*. *Ganong's review of medical physiology*.

Basser, P. J., Mattiello, J., & Le Bihan, D. (1994). MR diffusion tensor spectroscopy and imaging. *Biophysical Journal*, *66*(1), 259–267. https://doi.org/10.1016/S0006-3495(94)80775-1

Baudrexel, S., Witte, T., Seifried, C., von Wegner, F., Beissner, F., Klein, J. C., … Hilker, R. (2011). Resting state fMRI reveals increased subthalamic nucleus-motor cortex connectivity in Parkinson's disease. *NeuroImage*, *55*(4), 1728–1738. https://doi.org/10.1016/j.neuroimage.2011.01.017

Behrens, T. E. J., Johansen-Berg, H., Woolrich, M. W., Smith, S. M., Wheeler-Kingshott, C. a M., Boulby, P. a, … Matthews, P. M. (2003). Non-invasive mapping of connections between human thalamus and cortex using diffusion imaging. *Nature Neuroscience*, *6*(7), 750–757. https://doi.org/10.1227/01.NEU.0000309595.77090.89

Behrens, T. E. J., Woolrich, M. W., Jenkinson, M., Johansen-Berg, H., Nunes, R. G., Clare, S., … Smith, S. M. (2003). Characterization and propagation of uncertainty in diffusion-weighted MR imaging. *Magnetic Resonance in Medicine : Official Journal of the Society of Magnetic Resonance in Medicine / Society of Magnetic Resonance in Medicine*, *50*(5), 1077–88. https://doi.org/10.1002/mrm.10609

Benabid, A. L., Koudsie, A., Benazzouz, A., Le Bas, J.-F., & Pollak, P. (2002). Imaging of subthalamic nucleus and ventralis intermedius of the thalamus. *Movement Disorders :*

Official Journal of the Movement Disorder Society, *17 Suppl 3*, S123-9. https://doi.org/10.1002/mds.10153

Benabid, A., Pollak, P., Gao, D., Hoffmann, D., Limousin, P., Gay, E., … Benazzouz, A. (1996). Chronic electrical stimulation of the ventralis intermedius nucleus of the thalamus as a treatment of movement disorders. *Journal of Neurosurgery*, *84*, 203–214. https://doi.org/10.3171/jns.1996.84.2.0203

Biswal, B., Yetkin, F. Z., Haughton, V. M., & Hyde, J. S. (1995). Functional connectivity in the motor cortex of resting human brain using echo-planar MRI. *Magnetic Resonance in Medicine : Official Journal of the Society of Magnetic Resonance in Medicine / Society of Magnetic Resonance in Medicine*, *34*(4), 537–41. https://doi.org/10.1002/mrm.1910340409

Boecker, H., & Brooks, D. J. (1998). Functional imaging of tremor. *Movement Disorders : Official Journal of the Movement Disorder Society*, *13 Suppl 3*, 64–72.

Boecker, H., Wills, A. J., Ceballos-Baumann, A., Samuel, M., Thomas, D. G. T., Marsden, C. D., & Brooks, D. J. (1997). Stereotactic thalamotomy in tremor-dominant Parkinson's disease: An H215O PET motor activation study. *Annals of Neurology*, *41*(1), 108–111. https://doi.org/10.1002/ana.410410118

Bornstein, R. A., Schwarzkopf, S. B., Olson, S. C., & Nasrallah, H. A. (1992). Third-ventricle enlargement and neuropsychological deficit in schizophrenia. *Biological Psychiatry*, *31*(9), 954–961. https://doi.org/10.1016/0006-3223(92)90121-F

Braak, H., & Del Tredici, K. (2008). Invited Article: Nervous system pathology in sporadic Parkinson disease. *Neurology*, *70*(20), 1916–1925. https://doi.org/10.1212/01.wnl.0000312279.49272.9f

Buxton, R. B. (2009). *Introduction to Functional Magnetic Resonance Imaging: Principles and Techniques* (2nd ed.). Cambridge, UK: Cambridge University Press.

Cagnan, H., Little, S., Foltynie, T., Limousin, P., Zrinzo, L., Hariz, M., … Brown, P. (2014). The nature of tremor circuits in parkinsonian and essential tremor. *Brain*, *137*(12), 3223–3234. https://doi.org/10.1093/brain/awu250

Ceballos-Baumann, A. O. (2003). Functional imaging in Parkinson's disease: activation studies with PET, fMRI and SPECT. *Journal of Neurology*, *250 Suppl*, I15-23. https://doi.org/10.1007/s00415-003-1103-1

Chakravarty, M. M., Bertrand, G., Hodge, C. P., Sadikot, A. F., & Collins, D. L. (2006). The

creation of a brain atlas for image guided neurosurgery using serial histological data. *NeuroImage*, *30*(2), 359–376. https://doi.org/10.1016/j.neuroimage.2005.09.041

Chakravarty, M. M., Broadbent, S., Rosa-Neto, P., Lambert, C. M., & Collins, D. L. (2009). Design, construction, and validation of an MRI-compatible vibrotactile stimulator intended for clinical use. *Journal of Neuroscience Methods*, *184*(1), 129–135. https://doi.org/10.1016/j.jneumeth.2009.07.018

Coenen, V. A., Allert, N., & Mädler, B. (2011). A role of diffusion tensor imaging fiber tracking in deep brain stimulation surgery: DBS of the dentato-rubro-thalamic tract (drt) for the treatment of therapy-refractory tremor. *Acta Neurochirurgica*, *153*(8), 1579–1585. https://doi.org/10.1007/s00701-011-1036-z

Cole, D. M., Smith, S. M., & Beckmann, C. F. (2010). Advances and pitfalls in the analysis and interpretation of resting-state FMRI data. *Frontiers in Systems Neuroscience*, *4*(April), 8. https://doi.org/10.3389/fnsys.2010.00008

Damoiseaux, J. S., & Greicius, M. D. (2009). Greater than the sum of its parts: a review of studies combining structural connectivity and resting-state functional connectivity. *Brain Structure & Function*, *213*(6), 525–533. https://doi.org/10.1007/s00429-009-0208-6

DeMeyer, M. K., Gilmore, R., DeMeyer, W. E., Hendrie, H., Edwards, M., & Franco, J. N. (1984). Third Ventricle Size and Ventricular/Brain Ratio in Treatment-Resistant Psychiatric Patients. *Journal of Operational Psychiatry*, *15*, 2–8.

Deng, H., Le, W., & Jankovic, J. (2007). Genetics of essential tremor. *Brain*, *130*, 1456–1464. https://doi.org/10.1016/j.parkreldis.2015.09.022

Deuschl, G., Bain, P., Brin, M., Agid, Y., Benabid, L., Benecke, R., … Toloso, E. (1998). Consensus Statement of the Movement Disorder Society on Tremor. *Mov. Disord.*, *13*(S3), 2–23. https://doi.org/10.1002/mds.870131303

Duval, C., Daneault, J. F., Hutchison, W. D., & Sadikot, A. F. (2016). A brain network model explaining tremor in Parkinson's disease. *Neurobiology of Disease*, *85*, 49–59. https://doi.org/10.1016/j.nbd.2015.10.009

Elble, R. J. (2013). Defining dystonic tremor. *Current Neuropharmacology*, *11*(1), 48–52. https://doi.org/10.2174/157015913804999478

Fahn, S., Tolosa, E., & Marín, C. (1988). Clinical Rating Scale for Tremor. *Parkinson's Disease and Movement Disorders*, (November), 225–34. Retrieved from

http://www.ncbi.nlm.nih.gov/pubmed/3315156

Fan, Y., Nickerson, L., Li, H., Ma, Y., Lyu, B., Miao, X., … Gao, J.-H. (2015). Functional connectivity-based parcellation of the thalamus: An unsupervised clustering method and its validity investigation. *Brain Connectivity*, *XX*(Xx), 1–11. https://doi.org/10.1089/brain.2015.0338

Fang, W., Chen, H., Wang, H., Zhang, H., Puneet, M., Liu, M., … Lu, X. (2015). Essential tremor is associated with disruption of functional connectivity in the ventral intermediate Nucleus-Motor Cortex-Cerebellum circuit. *Human Brain Mapping*, *0*(1), n/a-n/a. https://doi.org/10.1002/hbm.23024

Felten, D. L., O'Banion, M. K., & Maida, M. S. (2015). *Netter's atlas of neuroscience*. Elsevier Health Sciences.

Fischl, B. (2012). FreeSurfer, *62*(2), 774–781. https://doi.org/10.1016/j.neuroimage.2012.01.021.FreeSurfer

Folstein, M. F., Folstein, S. E., & McHugh, P. R. (1975). "Mini-mental state". A practical method for grading the cognitive state of patients for the clinician. *Journal of Psychiatric Research*, *12*(3), 189–198. https://doi.org/10.1016/0022-3956(75)90026-6

Frighetto, L., Bizzi, J., & Oppitz, P. (2011). Stereotactic Radiosurgery for Movement Disorders BT - Shaped Beam Radiosurgery: State of the Art. In A. A. F. De Salles, A. Gorgulho, N. Agazaryan, B. Slotman, M. Selch, A. J. Burwick, & R. Schulz (Eds.) (pp. 209–218). Berlin, Heidelberg: Springer Berlin Heidelberg. https://doi.org/10.1007/978-3-642-11151-8_18

Garonzik, I. M., Hua, S. E., Ohara, S., & Lenz, F. A. (2002). Intraoperative microelectrode and semi-microelectrode recording during the physiological localization of the thalamic nucleus ventral intermediate. *Movement Disorders*, *17*(SUPPL. 3). https://doi.org/10.1002/mds.10155

Ghaderi, H., Sadikot, A., Campbell, J., & Pike, G. B. (2012). Automatic , rapid , non-invasive and precise localization of thalamic nuclei for Deep Brain Stimulation (DBS) surgery using a combination of Diffusion and Functional MRI, *45*(2), 2012.

Ghaderi, H., Sadikot, A. F., & Pike, G. B. (2014). Functional Target localization for neurosurgery: task based fMRI versus resting state fMRI study. *ISMRM 2014 Abstract*, (Appendix A), 14–15. https://doi.org/10.1016/j.neuroimage.2005.09.041.15

Gibrat, C., Saint-Pierre, M., Bousquet, M., Levesque, D., Rouillard, C., & Cicchetti, F. (2009).

Differences between subacute and chronic MPTP mice models: Investigation of dopaminergic neuronal degeneration and alpha-synuclein inclusions. *Journal of Neurochemistry*, *109*(5), 1469–1482. https://doi.org/10.1111/j.1471-4159.2009.06072.x

Goetz, C. G., Fahn, S., Martinez-Martin, P., Poewe, W., Sampaio, C., Stebbins, G. T., … LaPelle, N. (2007). Movement disorder society-sponsored revision of the unified Parkinson's disease rating scale (MDS-UPDRS): Process, format, and clinimetric testing plan. *Movement Disorders*, *22*(1), 41–47. https://doi.org/10.1002/mds.21198

Guyton, A. C., & Hall, J. E. (2006). *Texbook of Medical Physiology*. Elsevier Inc. https://doi.org/10.1136/pgmj.51.599.683-c

Hale, J. R., Mayhew, S. D., Mullinger, K. J., Wilson, R. S., Arvanitis, T. N., Francis, S. T., & Bagshaw, A. P. (2015). Comparison of functional thalamic segmentation from seed-based analysis and ICA. *NeuroImage*, *114*, 448–465. https://doi.org/10.1016/j.neuroimage.2015.04.027

Haug, G. (1978). Age and Sex Dependence of the Size of Normal Ventricles on Computed Tomography. *Neuroradiology*, *204*(1977), 201–204.

Horn, A., Kühn, A. A., Merkl, A., Shih, L., Alterman, R., & Fox, M. (2017). Probabilistic conversion of neurosurgical DBS electrode coordinates into MNI space. *NeuroImage*, *150*(August 2016), 395–404. https://doi.org/10.1016/j.neuroimage.2017.02.004

Hua, S. E. (2004). Posture-Related Oscillations in Human Cerebellar Thalamus in Essential Tremor Are Enabled by Voluntary Motor Circuits. *Journal of Neurophysiology*, *93*(1), 117–127. https://doi.org/10.1152/jn.00527.2004

Hyam, J. A., Owen, S. L. F., Kringelbach, M. L., Jenkinson, N., Stein, J. F., Green, A. L., & Aziz, T. Z. (2012). Contrasting connectivity of the ventralis intermedius and ventralis oralis posterior nuclei of the motor thalamus demonstrated by probabilistic tractography. *Neurosurgery*, *70*(1), 162–169. https://doi.org/10.1227/NEU.0b013e3182262c9a

Jankovic, J. (2008). Parkinson's disease: clinical features and diagnosis. *Journal of Neurology, Neurosurgery & Psychiatry*, *79*(4), 368–376. https://doi.org/10.1136/jnnp.2007.131045

Ji, B., Li, Z., Li, K., Li, L., Langley, J., Shen, H., … Hu, X. (2016). Dynamic thalamus parcellation from resting-state fMRI data. *Human Brain Mapping*, *37*(3), 954–967. https://doi.org/10.1002/hbm.23079

Johansen-Berg, H., Behrens, T. E. J., Sillery, E., Ciccarelli, O., Thompson, A. J., Smith, S. M., &

Matthews, P. M. (2005). Functional-anatomical validation and individual variation of diffusion tractography-based segmentation of the human thalamus. *Cerebral Cortex*, *15*(1), 31–39. https://doi.org/10.1093/cercor/bhh105

Jones, E. G. (2007). *The Thalamus*. New York: Springer Science + Business Media, LLC. https://doi.org/10.1007/978-1-4615-1749-8

Kincses, Z. T., Szabó, N., Valálik, I., Kopniczky, Z., Dézsi, L., Klivényi, P., … Vécsei, L. (2012). Target identification for stereotactic thalamotomy using diffusion tractography. *PLoS ONE*, *7*(1). https://doi.org/10.1371/journal.pone.0029969

Komisaruk, B. R., Wise, N., Frangos, E., Liu, W.-C., Allen, K., & Brody, S. (2011). Women's clitoris, vagina and cervix mapped on the sensory cortex: fMRI evidence. *J Sex Med.*, *8*(10), 2822–2830. https://doi.org/10.1111/j.1743-6109.2011.02388.x.Women

Kringelbach, M. L., Jenkinson, N., Owen, S. L. F., & Aziz, T. Z. (2007). Translational principles of deep brain stimulation. *Nature Reviews. Neuroscience*, *8*(8), 623–635. https://doi.org/10.1038/nrn2196

Kultas-Ilinsky, K., & Ilinskii, I. A. (2001). *Basal Ganglia and Thalamus in Health and Movement Disorders*. Springer Science + Business Media, LLC. https://doi.org/10.1007/978-1-4615-1235-6

Larson, P. S. (2014). Deep Brain Stimulation for Movement Disorders. *Neurotherapeutics*, *11*(3), 465–474. https://doi.org/10.1007/s13311-014-0274-1

Lenglet, C., Abosch, A., Yacoub, E., De Martino, F., Sapiro, G., & Harel, N. (2012). Comprehensive in vivo Mapping of the Human Basal Ganglia and Thalamic Connectome in Individuals Using 7T MRI. *PLoS ONE*, *7*(1), e29153. https://doi.org/10.1371/journal.pone.0029153

Lipsman, N., Schwartz, M. L., Huang, Y., Lee, L., Sankar, T., Chapman, M., … Lozano, A. M. (2013). MR-guided focused ultrasound thalamotomy for essential tremor: A proof-of-concept study. *The Lancet Neurology*, *12*(5), 462–468. https://doi.org/10.1016/S1474-4422(13)70048-6

Louis, E. D., & Ferreira, J. J. (2010). How common is the most common adult movement disorder? Update on the worldwide prevalence of essential tremor. *Movement Disorders*, *25*(5), 534–541. https://doi.org/10.1002/mds.22838

Lozano, A. M., & Mahant, N. (2004). Deep brain stimulation surgery for Parkinson's disease:

Mechanisms and consequences. *Parkinsonism and Related Disorders*, *10*, 49–57. https://doi.org/10.1016/j.parkreldis.2003.12.006

Luxenberg, J., Haxby, J., Creasy, H., Sundaram, M., & Rapoport, S. (1987). Rate of ventricular enlargement in dementia of the Alzheimer type correlates with rate of neuropsychological deterioration. *Neurology*, *2*(37), 1135–1140.

Magnotta, V. a, Gold, S., Andreasen, N. C., Ehrhardt, J. C., & Yuh, W. T. (2000). Visualization of subthalamic nuclei with cortex attenuated inversion recovery MR imaging. *NeuroImage*, *11*(4), 341–6. https://doi.org/10.1006/nimg.2000.0552

Miner, R. C. (2017). *Image-Guided Neurosurgery*. *Journal of Medical Imaging and Radiation Sciences* (Vol. 48). https://doi.org/10.1016/j.jmir.2017.06.005

Mitrofanis, J. (2005). Some certainty for the "zone of uncertainty"? Exploring the function of the zona incerta. *Neuroscience*, *130*(1), 1–15. https://doi.org/10.1016/j.neuroscience.2004.08.017

Morel, A. (2007). Stereotactic Atlas of the Human Thalamus and Basal Ganglia, *1*. https://doi.org/10.1017/CBO9781107415324.004

Müller, M., Esser, R., Kötter, K., Voss, J., Müller, A., & Stellmes, P. (2013). Third ventricular enlargement in early stages of multiple sclerosis is a predictor of motor and neuropsychological deficits: A cross-sectional study. *BMJ Open*, *3*(9), 1–6. https://doi.org/10.1136/bmjopen-2013-003582

Murray, C. J. (2015). Global, regional, and national age–sex specific all-cause and cause-specific mortality for 240 causes of death, 1990–2013: a systematic analysis for the Global Burden of Disease Study 2013. https://doi.org/10.1016/ S0140-6736(14)61682-2

Nelson, S., Andy, O., & Foshee, D. (1964). Third Ventricle Size in Patients with Movement Disorders. *Confin. Neurol.*, *24*, 308–313.

Pahwa, R., Factor, P., Lyons, K., Ondo, W., Gronseth, G., Bronte-Stewart, H., … Weiner, W. (2006). Practice parameter: treatment of Parkinson disease with motor fluctuations and dyskinesia (an evidence-based review). Report of the Quality Standards Subcommittee of the American Academy of Neurology. *American Academy of Neurology*, *66*, 983–995.

Papavassiliou, E., Rau, G., Heath, S., Abosch, A., Barbaro, N. M., Larson, P. S., … Starr, P. A. (2004). Thalamic Deep Brain Stimulation for Essential Tremor: Relation of Lead Location to Outcome. *Neurosurgery*, *54*(5), 1120–1130.

https://doi.org/10.1227/01.NEU.0000134764.76223.4B

Perlmutter, J. S., & Mink, J. W. (2006). Deep brain stimulation. *Annual Review of Neuroscience*, *29*, 229–257. https://doi.org/10.1146/annurev.neuro.29.051605.112824

Picillo, M., Moro, E., Edwards, M., Di Lazzaro, V., Lozano, A. M., & Fasano, A. (2015). Subdural continuous theta burst stimulation of the motor cortex in essential tremor. *Brain Stimulation*, *8*(4), 840–842. https://doi.org/10.1016/j.brs.2015.05.003

Pierpaoli, C., Jezzard, P., Basser, P. J., Barnett, A., & Di Chiro, G. (1996). Diffusion tensor MR imaging of the human brain. *Radiology*, *201*(3), 637–648. https://doi.org/10.1148/radiology.201.3.8939209

Plaha, P., Khan, S., & Gill, S. S. (2008). Bilateral stimulation of the caudal zona incerta nucleus for tremor control. *Journal of Neurology, Neurosurgery and Psychiatry*, *79*(5), 504–513. https://doi.org/10.1136/jnnp.2006.112334

Pouratian, N., Zheng, Z., Bari, A. A., Behnke, E., Elias, W. J., & DeSalles, A. A. F. (2011). Multi-institutional evaluation of deep brain stimulation targeting using probabilistic connectivity-based thalamic segmentation. *Journal of Neurosurgery*, *115*(5), 995–1004. https://doi.org/10.3171/2011.7.JNS11250

Pruim, R. H. R., Mennes, M., Rooij, D. Van, Llera, A., Buitelaar, J. K., & Beckmann, C. F. (2015). NeuroImage ICA-AROMA : A robust ICA-based strategy for removing motion artifacts from fMRI data. *NeuroImage*, *112*, 267–277. https://doi.org/10.1016/j.neuroimage.2015.02.064

Purves, D., Augustine, G. J., Fitzpatrick, D., Katz, L. C., LaMantia, A.-S., McNamara, J. O., & Williams, S. M. (2001). The Somatic Sensory Cortex. Retrieved from https://www.ncbi.nlm.nih.gov/books/NBK11153/

Redfern, R. M., & Ruskin, J. (1989). History of stereotactic surgery for parkinson's disease. *British Journal of Neurosurgery*, *3*(3), 271–304. https://doi.org/10.3109/02688698909002807

Rodriguez-Oroz, M. C., Obeso, J. A., Lang, A. E., Houeto, J.-L., Pollak, P., Rehncrona, S., … Van Blercom, N. (2005). Bilateral deep brain stimulation in Parkinson's disease: a multicentre study with 4 years follow-up. *Brain*, *128*(10), 2240–2249. https://doi.org/10.1093/brain/awh571

Rodriguez, M. C., Guridi, O. J., Alvarez, L., Mewes, K., Macias, R., Vitek, J., … Obeso, J. a. (1998). The subthalamic nucleus and tremor in Parkinson's disease. *Movement Disorders : Official Journal of the Movement Disorder Society*, *13 Suppl 3*, 111–118.

https://doi.org/9827606

Rohani, M., & Fasano, A. (2017). Focused Ultrasound for Essential Tremor: Review of the Evidence and Discussion of Current Hurdles. *Tremor and Other Hyperkinetic Movements (New York, N.Y.)*, *7*, 462. https://doi.org/10.7916/D8Z89JN1

Sammartino, F., Krishna, V., King, N. K. K., Lozano, A. M., Schwartz, M. L., Huang, Y., & Hodaie, M. (2016). Tractography-Based Ventral Intermediate Nucleus Targeting: Novel Methodology and Intraoperative Validation. *Movement Disorders*, *31*(8), 1217–1225. https://doi.org/10.1002/mds.26633

Scahill, R. I., Frost, C., Jemkins, R., Withwell, Je. L., Rossor, M. N., & Fox, N. C. (2003). A longitudinal study of brain volume changes in normal aging using serial registered magnetic resonance imaging. *Archives of Neurology*, *60*(7), 989–994. https://doi.org/10.1001/archneur.60.7.989

Shahed, J., & Jankovic, J. (2007). Exploring the relationship between essential tremor and Parkinson's disease. *Parkinsonism & Related Disorders*, *13*(2), 67–76. https://doi.org/10.1016/j.parkreldis.2006.05.033

Singleton, A. B., Farrer, M. J., & Bonifati, V. (2013). The genetics of Parkinson's disease: Progress and therapeutic implications. *Movement Disorders*, *28*(1), 14–23. https://doi.org/10.1002/mds.25249

Smith, S., Jenkinson, M., Woolrich, M., Beckmann, C., Behrens, T., Johansen-Berg, H., … Matthews, P. M. (2004). Advances in functional and structural MR image analysis and implementation as FSL. *NeuroImage*, *23*(SUPPL. 1), 208–219. https://doi.org/10.1016/j.neuroimage.2004.07.051

Soares, J. M., Marques, P., Alves, V., & Sousa, N. (2013). A hitchhiker's guide to diffusion tensor imaging. *Frontiers in Neuroscience*, *7*(7 MAR), 1–14. https://doi.org/10.3389/fnins.2013.00031

Sommer, M. A. (2003). The role of the thalamus in motor control. *Current Opinion in Neurobiology*, *13*(6), 663–670. https://doi.org/10.1016/j.conb.2003.10.014

Sprawls, P. (2000). *Magnetic resonance imaging: principles, methods, and techniques*. Medical Physics Publishing.

Stough, J. V., Glaister, J., Ye, C., Ying, S. H., Prince, J. L., & Carass, A. (2014). Automatic method for thalamus parcellation using multi-modal feature classification. *Lecture Notes in Computer*

Science (Including Subseries Lecture Notes in Artificial Intelligence and Lecture Notes in Bioinformatics), *8675 LNCS*(PART 3), 169–176. https://doi.org/10.1007/978-3-319-10443-0_22

Sudhyadhom, A., Haq, I. U., Foote, K. D., Okun, M. S., & Bova, F. J. (2009). A high resolution and high contrast MRI for differentiation of subcortical structures for DBS targeting: The Fast Gray Matter Acquisition T1 Inversion Recovery (FGATIR). *NeuroImage*, *47*(SUPPL. 2), T44–T52. https://doi.org/10.1016/j.neuroimage.2009.04.018

Sullivan, E. V., Rosenbloom, M., Serventi, K. L., & Pfefferbaum, A. (2004). Effects of age and sex on volumes of the thalamus, pons, and cortex. *Neurobiology of Aging*, *25*(2), 185–192. https://doi.org/10.1016/S0197-4580(03)00044-7

Tang, Y., Hojatkashani, C., Dinov, I. D., Sun, B., Fan, L., Lin, X., … Toga, A. W. (2010). The construction of a Chinese MRI brain atlas: A morphometric comparison study between Chinese and Caucasian cohorts. *NeuroImage*, *51*(1), 33–41. https://doi.org/10.1016/j.neuroimage.2010.01.111

Team, R. C. (2013). R: A language and environment for statistical computing.

Thambisetty, M., Wan, J., Carass, A., An, Y., Prince, J. L., & Resnick, S. M. (2010). Longitudinal changes in cortical thickness associated with normal aging. *NeuroImage*, *52*(4), 1215–1223. https://doi.org/10.1016/j.neuroimage.2010.04.258

Thenganatt, M. A., & Jankovic, J. (2016). The relationship between essential tremor and Parkinson's disease. *Parkinsonism and Related Disorders*, *22*, S162–S165. https://doi.org/10.1016/j.parkreldis.2015.09.032

Vassal, F., Coste, J., Derost, P., Mendes, V., Gabrillargues, J., Nuti, C., … Lemaire, J. J. (2012). Direct stereotactic targeting of the ventrointermediate nucleus of the thalamus based on anatomic 1.5-T MRI mapping with a white matter attenuated inversion recovery (WAIR) sequence. *Brain Stimulation*, *5*(4), 625–633. https://doi.org/10.1016/j.brs.2011.10.007

Vincent, K., Moore, J., Kennedy, S., & Tracey, I. (2009). Blood oxygenation level dependent functional magnetic resonance imaging: Current and potential uses in obstetrics and gynaecology. *BJOG: An International Journal of Obstetrics and Gynaecology*, *116*(2), 240–246. https://doi.org/10.1111/j.1471-0528.2008.01993.x

Vitek, J. L., Ashe, J., DeLong, M. R., & Alexander, G. E. (1994). Physiologic properties and somatotopic organization of the primate motor thalamus. *Journal of Neurophysiology*, *71*(4),

1498–1513.

Wiegell, M. R., Tuch, D. S., Larsson, H. B. W., & Wedeen, V. J. (2003). Automatic segmentation of thalamic nuclei from diffusion tensor magnetic resonance imaging. *NeuroImage*, *19*(2 Pt 1), 391–401. https://doi.org/10.1016/S1053-8119(03)00044-2

Woolrich, M. W., Ripley, B. D., Brady, M., & Smith, S. M. (2001). Temporal autocorrelation in univariate linear modeling of FMRI data. *NeuroImage*, *14*(6), 1370–1386. https://doi.org/10.1006/nimg.2001.0931

Yamada, K., Akazawa, K., Yuen, S., Goto, M., Matsushima, S., Takahata, A., … Nishimura, T. (2010). MR imaging of ventral thalamic nuclei. *American Journal of Neuroradiology*, *31*(4), 732–735. https://doi.org/10.3174/ajnr.A1870

Yamamoto, H., Kamegaya, E., Sawada, W., Hasegawa, R., Yamamoto, T., Hagino, Y., … Ikeda, K. (2013). Involvement of the N-methyl-d-aspartate receptor GluN2D subunit in phencyclidine-induced motor impairment, gene expression, and increased Fos immunoreactivity. *Molecular Brain*, *6*(1). https://doi.org/10.1186/1756-6606-6-56

Yousry, T. A., Schmid, U. D., Alkadhi, H., Schmidt, D., Peraud, A., Buettner, A., & Winkler, P. (1997). Localization of the motor hand area to a knob on the precentral gyrus. A new landmark. *Brain*, *120*(1), 141–157. https://doi.org/10.1093/brain/120.1.141

Zesiewicz, T. A., Elble, R., Louis, E. D., Ondo, W. G., Gronseth, G. S., & Weiner, W. J. (2008). Practice Parameter : Therapies for essential tremor - Report of the Quality Standards Subcommittee of the American Academy of Neurology.

Zhang, D., Snyder, A., Fox, M., Sansbury, M., Shimony, J., & Raichle, M. (2008). Intrinsic functional relations between human cerebral cortex and thalamus. *Journal of Neurophysiology*, *100*(4), 1740–1748. https://doi.org/10.1152/jn.90463.2008

Zhang, D., Snyder, A., Shimony, J., Fox, M., & Raichle, M. (2010). Noninvasive Functional and Structural Connectivity Mapping of the Human Thalamocortical System. *Cerebral Cortex*, *20*(5), 1187–1194. https://doi.org/10.1093/cercor/bhp182